

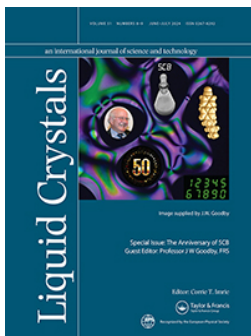
CRUICKSHANK, E., STRACHAN, G.J., THAPA, K., POCIECHA, D., SALAMOŃCZYK, M., STOREY, J.M.D., GORECKA, E., LAVRENTOVICH, O. and IMRIE, C.T. 2024. Cyanobiphenyl-based liquid crystal dimers and the twist-bend nematic phase: on the role played by the length and parity of the spacer. *Liquid crystals* [online], 51(8-9), pages 1446-1470. Available from: <https://doi.org/10.1080/02678292.2024.2381570>

Cyanobiphenyl-based liquid crystal dimers and the twist-bend nematic phase: on the role played by the length and parity of the spacer.

CRUICKSHANK, E., STRACHAN, G.J., THAPA, K., POCIECHA, D., SALAMOŃCZYK, M., STOREY, J.M.D., GORECKA, E., LAVRENTOVICH, O. and IMRIE, C.T.

2024

© 2024 The Author(s). Published by Informa UK Limited, trading as Taylor & Francis Group.
Supplementary materials are appended after the main text of this document.



Cyanobiphenyl-based liquid crystal dimers and the twist-bend nematic phase: on the role played by the length and parity of the spacer

Ewan Cruickshank, Grant J Strachan, Kamal Thapa, Damian Pocięcha, Mirosław Salamończyk, John M D Storey, Ewa Gorecka, Oleg Lavrentovich & Corrie T Imrie

To cite this article: Ewan Cruickshank, Grant J Strachan, Kamal Thapa, Damian Pocięcha, Mirosław Salamończyk, John M D Storey, Ewa Gorecka, Oleg Lavrentovich & Corrie T Imrie (2024) Cyanobiphenyl-based liquid crystal dimers and the twist-bend nematic phase: on the role played by the length and parity of the spacer, *Liquid Crystals*, 51:8-9, 1446-1470, DOI: [10.1080/02678292.2024.2381570](https://doi.org/10.1080/02678292.2024.2381570)

To link to this article: <https://doi.org/10.1080/02678292.2024.2381570>



© 2024 The Author(s). Published by Informa UK Limited, trading as Taylor & Francis Group.



[View supplementary material](#)



Published online: 19 Aug 2024.



[Submit your article to this journal](#)



Article views: 638



[View related articles](#)



[View Crossmark data](#)

Cyanobiphenyl-based liquid crystal dimers and the twist-bend nematic phase: on the role played by the length and parity of the spacer

Ewan Cruickshank^a, Grant J Strachan^a, Kamal Thapa^{b,c}, Damian Pocięcha^d, Mirosław Salamończyk^d, John M D Storey^a, Ewa Gorecka^d, Oleg Lavrentovich^{b,c,e} and Corrie T Imrie^a

^aDepartment of Chemistry, School of Natural and Computing Sciences, University of Aberdeen, Aberdeen, UK; ^bAdvanced Materials and Liquid Crystal Institute, Kent State University, Kent, OH, USA; ^cDepartment of Physics, Kent State University, Kent, OH, USA; ^dFaculty of Chemistry, University of Warsaw, Warsaw, Poland; ^eMaterials Science Graduate Program, Kent State University, Kent, OH, USA

ABSTRACT

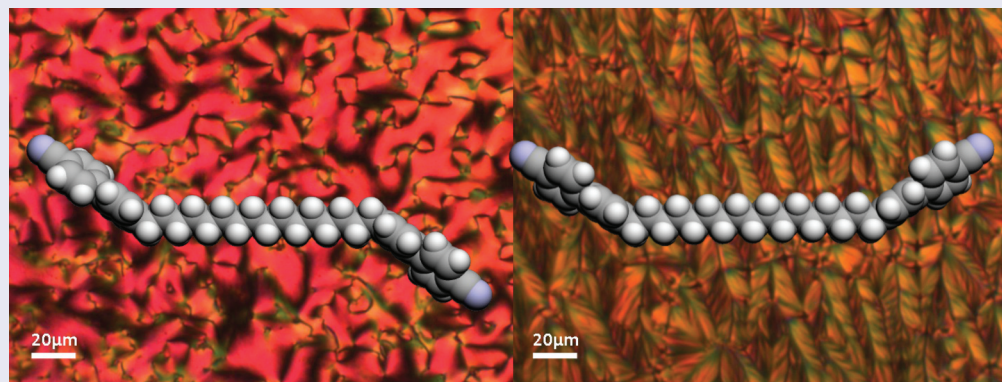
Six members of the 1,ω-bis(4-cyanobiphenyl-4'-yl) alkanes are reported and referred to as CB n CB in which $n = 1, 15, 16, 17, 19$ and 20 and indicates the number of methylene units in the spacer separating the two cyanobiphenyl units. The behaviour of CB3CB is revisited. The temperature dependence of the refractive indices, optical birefringence and dielectric permittivities measured in the nematic, N, phase for selected homologues are reported. The dimers with $n \geq 15$ showed an enantiotropic N phase, and for the odd members the twist-bend nematic, N_{TB}, phase was observed. CB3CB shows a direct N_{TB}-isotropic, I, transition, whereas for CB1CB a virtual N_{TB}-I transition is found. The temperature dependence of the bend elastic constant, K_{33} , measured in the oblique helicoidal cholesteric state formed by mixtures of CB n CB with a chiral additive S811, shows strong non-monotonous behaviour with a deep minimum near the transition point to the N_{TB} phase. The minimum value of K_{33} decreases as n increases. The long even members of the CB n CB series show similar values of T_{NI} to their odd-membered counterparts, but their estimated values of $T_{N_{TB}N}$ are considerably lower. This is attributed to molecular shape and its effect on K_{33} .

ARTICLE HISTORY

Received 7 March 2024

KEYWORDS

Twist-bend nematic phase; liquid crystal dimers; bend elastic constant; pitch length; helicoidal cholesteric phase; spacer



1. Introduction

Over a decade has now passed since the first unambiguous assignment of the twist-bend nematic, N_{TB}, phase was made [1–3], and some 50 years since Meyer predicted its existence [4] and over 20 years since it was predicted independently by Dozov [5], both using symmetry arguments. A range of molecular structures have now been shown to exhibit the N_{TB} phase including odd-membered liquid crystal dimers [6–27] and higher oligomers [28–35], bent-core liquid crystals [36,37],

hydrogen-bonded supramolecular systems [38–42] and polymeric liquid crystals [43]. Recently, an even-membered dimer containing a disulphide link in the spacer has been reported to exhibit the N_{TB} phase [44]. The common feature to each of these classes of materials is molecular bend, and this is wholly consistent with Dozov's seminal work [5]. He argued that bent molecules have a strong natural tendency to pack into bent structures, but, given that pure uniform bend is not allowed in nature, it must be accompanied by another

CONTACT Corrie T Imrie  c.t.imrie@abdn.ac.uk

 Supplemental data for this article can be accessed online at <https://doi.org/10.1080/02678292.2024.2381570>

© 2024 The Author(s). Published by Informa UK Limited, trading as Taylor & Francis Group.

This is an Open Access article distributed under the terms of the Creative Commons Attribution-NonCommercial-NoDerivatives License (<http://creativecommons.org/licenses/by-nc-nd/4.0/>), which permits non-commercial re-use, distribution, and reproduction in any medium, provided the original work is properly cited, and is not altered, transformed, or built upon in any way. The terms on which this article has been published allow the posting of the Accepted Manuscript in a repository by the author(s) or with their consent.

local deformation of the director. In the case of twist, this gives rise to the N_{TB} phase in which the director forms a heliconical distribution in which it is tilted with respect to the helical axis. The pitch of this helix is very short and typically just a few molecular lengths. A particularly fascinating feature of the N_{TB} phase is spontaneous symmetry breaking in a fluid system composed of achiral molecules and without positional order. Given that the formation of chirality is spontaneous equal numbers of left- and right-handed helices would be expected and hence, macroscopically the phase is achiral. The chiral N_{TB} phase may be obtained in which the double degeneracy of the helical twist sense has been removed either by the addition of chiral dopants [45] or by the introduction of intrinsic molecular chirality [46–48]. Dozov also predicted the existence of twist-bend smectic phases [5] and these have also been found experimentally [49–54].

The experimental discovery of the N_{TB} phase was made using CB7CB, a member of the 1, ω -bis(4-cyanobiphenyl-4'-yl) alkanes, the CB_nCB series, see Figure 1(a). In CB7CB, seven methylene units separate the two cyanobiphenyl moieties, and this odd-membered spacer imparts the necessary molecular curvature to observe the N_{TB} phase. The CB_nCB series contains three of the most extensively studied twist-bend nematogens; specifically, CB7CB, CB9CB and CB11CB (see for recent examples [55–67]). More widely, the overwhelming majority of twist-bend nematogens reported in the literature have either seven, nine or eleven atoms separating the mesogenic units. The reasons for this are two-fold: firstly, moving to shorter odd-membered spacers accentuates the molecular bend and tends to reduce the liquid crystal transition temperatures with respect to the melting point, and strongly monotropic materials are obtained [21,68]. Secondly, and more pragmatically, moving to longer odd-membered spacers is synthetically rather challenging. The CB_nCB series is one of the most complete homologous series to be studied in terms of the spacer length, with

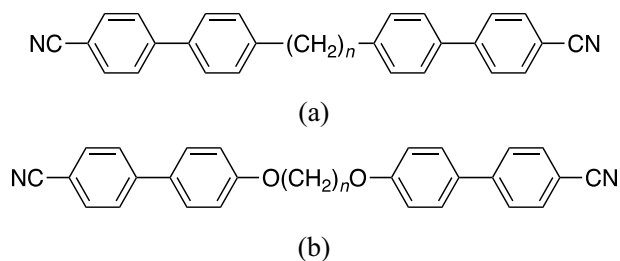


Figure 1. The general molecular structure of (a) the 1, ω -bis(4-cyanobiphenyl-4'-yl) alkanes, referred to as the CB_nCB series and (b) the 1, ω -bis(4-cyanobiphenyl-4'-yloxy) alkanes, the CBO_nOCB series. In both acronyms n refers to the number of methylene units in the flexible alkyl spacer.

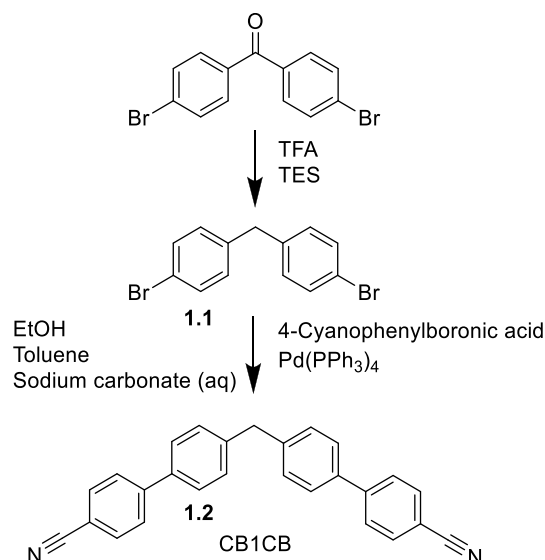
values of n reported of 3, 5–11 and 13 [67,69,70]. Key questions remain, however, such as, what happens to the tendency to form the N_{TB} phase when the spacer becomes even shorter, or indeed very long? To address these issues, here we report the synthesis and characterisation of new members of the CB_nCB series with $n = 1, 15, 17$ and 19 , and revisit the behaviour for $n = 3$. In order to establish the dependence of the formation of the N_{TB} phase on molecular shape, and specifically, the bend angle of the dimer, we compare the transitional properties of the CB_nCB series with those of the CBO_nOCB series [71,72], Figure 1(b). We also consider the difference in transitional behaviour between dimers having very long odd or even-membered spacers and report the synthesis and characterisation of members of the CB_nCB series with $n = 16$ and 20 .

To better understand the role of the spacer in determining the properties of these dimers, we also measure the temperature dependence of a number of material parameters, specifically the refractive indices, optical birefringence and dielectric permittivities of the N phase formed by members of the CB_nCB series with $n = 7, 9, 11, 13$ and 15 . We also investigate the bend elastic constants, K_{33} , for these homologues. The very low values of K_{33} found in the nematic phases of odd-membered dimers [73] have been attributed to the bent-shape adopted by these dimers [74] and drive the formation of both the N_{TB} phase and also of the so-called oblique helicoidal cholesteric state, Ch_{OH} . Unfortunately, direct measurements of K_{33} in the N phase of the CB_nCB dimers using the conventional technique involving a Frederiks transition in a homeotropic cell are problematic since the materials do not align homeotropically. Instead, we resort to measuring K_{33} in the chiral version of the N phase, the chiral nematic N^* phase in which the directors adopt a helical distribution and are perpendicular to the helical axis. When a N^* phase formed by an odd-membered dimer is acted upon by an electric field, the small value of K_{33} yields an oblique helicoidal Ch_{OH} state [64,75,76], in which the local director is now tilted to the helical axis [75,77]. In the Ch_{OH} state, the helical pitch P depends on K_{33} [75,78,79]; by measuring P using the electrically tuneable Bragg reflection of light, we may deduce K_{33} , as described previously [64,77].

2. Experimental

2.1. Synthetic methods

The synthesis of CB1CB is shown in Scheme 1. In the first step, 4,4'-dibromobenzophenone was



Scheme 1. Synthesis of CB1CB.

reduced using triethylsilane [67] to yield 1,1-bis(4-bromophenyl)ethane (1.1) that was subsequently reacted with 4-cyanophenylboronic acid in a Suzuki–Miyaura cross-coupling reaction [80] to give CB1CB (1.2).

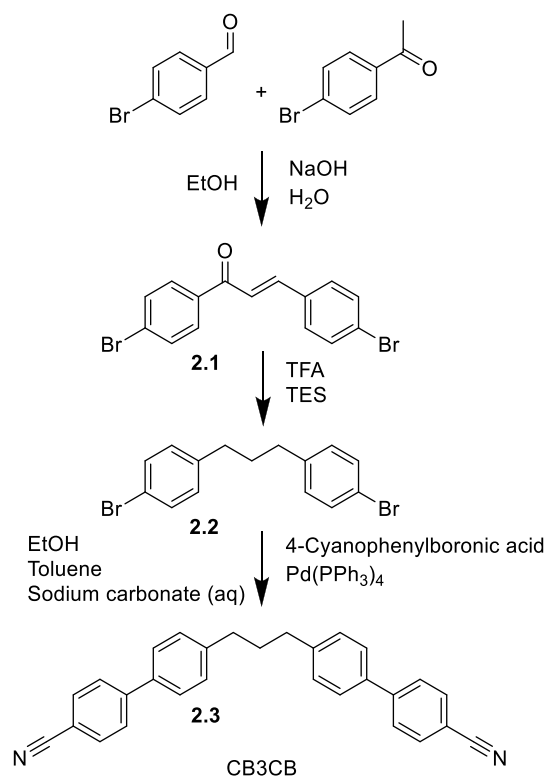
The synthesis of CB3CB followed the steps outlined in Scheme 2. In the first step, 2*E*-1,3-bis(4-bromophenyl)prop-2-en-1-one (2.1) was synthesised using a base catalysed aldol condensation between 4-bromobenzaldehyde and 4-bromoacetophenone [81]. 2.1 underwent a hydrosilane reduction [67] to form 1,3-bis(4-bromophenyl)propane (2.2) that was subsequently reacted with 4-cyanophenylboronic acid in a Suzuki–Miyaura cross-coupling reaction [80] to form the desired product, CB3CB (2.3).

The synthesis of the extended chain alkanedioic acids required for the syntheses of the CB n CB homologues with long spacers is shown in Scheme 3 and based on the procedure reported by Obaza and Smith [82]. The synthesis of the CB n CB homologues having long spacers is shown in Scheme 4 and described elsewhere by Paterson *et al.* [67]. A detailed description of the preparation of the members of the CB n CB series ($n = 1, 3, 15, 16, 17, 19, 20$), including the structural characterisation data for all intermediates and final products, is provided in the Supplementary Information.

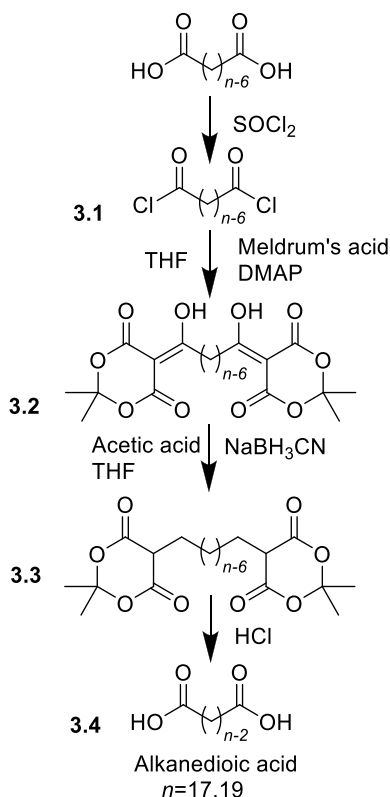
2.2. Thermal characterisation

Phase characterisation was performed by polarised light microscopy, using an Olympus BH2 polarising light microscope equipped with a Linkam TMS 92

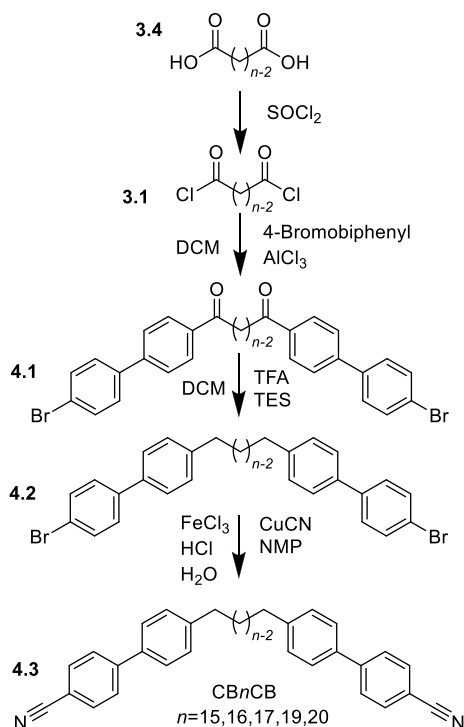
hot stage, a Lumenera Infinity Lite B CMOS camera, an Olympus IC20 LWD MSPlan 20 (0.40) objective and an Olympus 0.65 N.A. U-LWCD condenser, or a Zeiss AxioImager A2m microscope equipped with a Linkam THMS600 hot stage, a Canon EOS 90D DSLR camera, a Zeiss LD EC Epiplan-Neofluar M27 20× (0.22) objective and a Zeiss 0.9 N.A. achromatic-aplanatic universal Pol condenser. The untreated



Scheme 2. Synthesis of CB3CB.



Scheme 3. Synthesis of extended alkanedioic acids.



Scheme 4. Synthesis of the CBnCB series.

glass slides were approximately 0.17 mm thick. The cells treated for planar alignment were purchased from INSTEC, they were 2.9–3.5 μm thick and possessed transparent ITO electrodes.

The phase behaviour of the materials was studied by differential scanning calorimetry performed using a Mettler Toledo DSC1 or DSC3 differential scanning calorimeter equipped with TSO 801RO sample robots and calibrated using indium and zinc standards. Heating and cooling rates were 10 K min^{-1} , with a 3-min isotherm between either heating or cooling, and all samples were measured under a nitrogen atmosphere. Transition temperatures and associated enthalpy changes were extracted from the heating traces unless otherwise noted.

2.3. Molecular modelling

The geometric parameters of the CBnCB series were obtained using quantum mechanical DFT calculations with Gaussian09 software [83]. Optimisation of the molecular structures was carried out at the B3LYP/6-31 G(d) level. Visualisations of electronic surfaces and ball-and-stick models were generated from the optimised geometries using the GaussView 5 software [84]. The electronic surfaces were found with the cube-gen utility in GaussView by generating a total density cube using a SCF density matrix and course grid, overlaid by an ESP surface map. Visualisations of the space-filling models were produced post-optimisation using the QuteMol package [85].

2.4. Resonant X-ray scattering

The resonant X-ray scattering measurements were performed at the Advanced Light Source, Lawrence Berkeley National Laboratory on the soft X-ray beam line (11.0.1.2). The energy of the incident beam was tuned to the K-edge of carbon absorption (283 eV). Samples with thickness lower than 1 μm were prepared between SiN membranes. The scattering intensity was recorded using the Princeton PI-MTE CCD detector.

2.5. Refractive indices and birefringence of the N phase

The temperature dependence of the ordinary (n_o) and extra-ordinary (n_e) refractive indices was determined by investigating light interference in wedge cells [86]. The measurements were performed at the wavelengths 488 nm, 532 nm and 632.8 nm, using laser-line colour filters with a central bandwidth of 1 nm (Thorlabs, Inc.). The wedge cells of a small dihedral angle $<1^\circ$ were constructed using glass plates coated with a polyimide PI 2555, which is rubbed along the direction perpendicular to the thickness gradient to prevent

director deformations. The temperature dependencies of the birefringence, $\Delta n(T)$ were determined by measuring the optical retardance $\Gamma(T) = \Delta n(T)d$, in rubbed PI2555 planar cells with spacings $d = (3.9\text{--}4.2)$ μm , using a MicroImager (Hinds Instruments) at the wavelength 535 nm.

2.6. Dielectric anisotropy of the N phase

The dielectric permittivities were determined in thin rubbed PI2555 planar cells with spacing $d = (3.9\text{--}4.2)$ μm with square ITO electrodes of area 5 mm \times 5 mm at a frequency of 3 kHz, using capacitance measurements with a 4284A LCR meter (Hewlett Packard). The perpendicular permittivity $\epsilon_{\perp}(T)$ was measured at a low applied voltage of 0.1 V that does not perturb the homogeneous planar structure, whereas the parallel permittivity $\epsilon_{\parallel}(T)$ was measured in the same planar cell using an extrapolation method at high applied voltage that aligns the molecules perpendicularly to the electrodes [87].

2.7. Bend elastic constant in the oblique helicoidal state (Ch_{OH})

2.7.1. Preparation and characterisation of the chiral mixtures

The binary mixtures of the CB_nCB dimers, $n = 7, 9, 11, 13$ and 15, with the left-handed chiral additive (S)-2-octyl 4-[4-(hexyloxy)benzoyloxy] benzoate known as S811 (Tokyo Chemical Industry Co. Ltd., purity >98.0%, melting point 49°C), $\text{CB}_n\text{CB}:\text{S811} = 96:4$ (wt.%), were studied in ITO PI 2555 planar cells of spacing $d = (19.5\text{--}19.7)$ μm ; the larger spacing ensures strong Bragg reflection from the Ch_{OH} state. The phase transition temperatures were determined by observing the optical textures under the polarizing optical microscope, a Nikon OPTIPHOT2-POL (Nikon Instruments Inc.) equipped with an QImaging camera, on cooling from the isotropic phase at 0.1 K min^{-1} . The temperature was controlled using a HCS302 hot stage connected to a mK2000 controller (Instec, Inc.) with an accuracy of ± 0.01 K.

2.7.2. Bend elastic constant in the oblique helicoidal state (Ch_{OH})

The temperature dependencies of the bend elastic constant K_{33} for the dimers were measured in the oblique helicoidal state (Ch_{OH}) using the chiral mixtures described in section 2.7.1. The Ch_{OH} state was obtained by applying an external sinusoidal ac voltage of frequency 3 kHz to ITO-covered planar cells of spacing $d = (19.5\text{--}19.7)$ μm [75,76]. The ac sinusoidal signal was produced by a SDG 1032X (SIGLENT Technologies) waveform generator and

amplified by a 7602 M (KROHN-HITE Co.) voltage amplifier. The applied voltage was measured using a KEITHLEY 2000 multimeter. A tungsten halogen light source, LS-1 (360–2000 nm) and a USB2000 fibre optics spectrometer (both Ocean Insight) were used to characterise the Bragg reflection. The unpolarised light from the LS-1 light source was passed through a UV–VIS bifurcated optical fibre (200 μm diameter) and was incident normally on the Ch_{OH} cells. The superimposed reflected beam from the Ch_{OH} cells passed through the same bifurcated optical fibre and detected using the USB2000 spectrometer interfaced with OceanView spectroscopy software (Ocean Insight). The well-equilibrated reflection spectra at each temperature point of interest, above the $\text{N}^*-\text{N}_{\text{TB}}^*$ transition temperature, were recorded as a function of the applied electric field E .

3. Results and discussion

3.1. Phase behaviour

The transitional properties of the new members of the CB_nCB series reported here are listed in Table 1. All the long homologues ($n \geq 15$) exhibit an enantiotropic conventional nematic phase identified on the basis of the textures observed using polarised light microscopy. Specifically, when sandwiched between two untreated glass slides, a characteristic schlieren texture was observed containing both two- and four-point brush singularities and which flashed when subjected to mechanical stress, see Figure 2(a). On cooling the odd members ($n = 15, 17, 19$), a blocky schlieren texture developed, see Figure 2(b), and this was accompanied by the cessation of the optical flickering associated with director fluctuations in the N phase. These changes are characteristic of a $\text{N}-\text{N}_{\text{TB}}$ phase transition. For CB15CB, the N_{TB} phase is enantiotropic, whereas for CB17CB and CB19CB it is marginally monotropic in nature. The long even-membered homologues ($n = 16, 20$) show an enantiotropic conventional nematic phase and the absence of the N_{TB} phase is consistent with the widely held view that molecular curvature is a prerequisite for its observation. We return to this theme later.

The N_{TB} phase exhibited by CB15CB was also characterised using resonant soft X-ray scattering (RSoXS). The diffraction signal under the resonance condition is sensitive to the orientation of the molecules unlike conventional XRD. Figure 3(a) shows the temperature evolution of the resonant XRD signal recorded in the N_{TB} phase and Figure 3(b) the temperature dependence of the measured pitch length. The values of the pitch length decrease from around 300 Å at the $\text{N}_{\text{TB}}-\text{N}$

Table 1. Transition temperatures and associated scaled entropy changes for the CB n CB series.

n	$T_{Cr}/^{\circ}C$	$T_{N_{TB}N}/^{\circ}C$	$T_{N_{TB}I}/^{\circ}C$	$T_{NI}/^{\circ}C$	$\Delta S_{Cr}/R$	$\Delta S_{NI}/R$
1	206	–	–3 ^b	–	7.43	–
3	141	–	47 ^c	–	8.29	–
15	96	103	–	121	13.5	1.50
16	111	–	–	132	13.4	2.17
17	99	97 ^a	–	117	15.3	1.45
19	99	95 ^a	–	115	16.7	2.20
20	115	–	–	116	15.3	1.76 ^{a,d}

^aValues extracted from DSC cooling traces. ^bVirtual transition temperature estimated from a binary phase diagram with CB7CB. ^cMeasured using the polarised light microscope. ^dThe peak associated with the N-I transition overlaps that associated with crystallisation on cooling and with melting on heating, and this value underestimates $\Delta S_{NI}/R$.

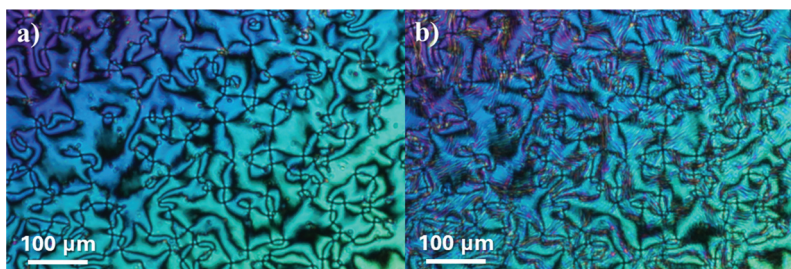


Figure 2. (Colour online) (a) The schlieren texture seen for the N phase ($T = 112^{\circ}C$) and (b) the blocky schlieren texture of the N_{TB} phase ($T = 94^{\circ}C$) observed for CB19CB.

transition to around 150 \AA on cooling. These values are much higher than previously measured for members of the CB n CB series; for example, the pitch length measured in the N_{TB} phase for CB7CB is around 80 \AA [2,3,88]. If we assume that the helical structure in the N_{TB} phase does not change with spacer length, then the increased pitch length may reflect, at least in part, the increase in molecular length from 26.2 \AA for CB7CB to 36.4 \AA for CB15CB. This increase in molecular length in itself, however, does not appear sufficiently large to account for a doubling of the pitch length. A strong dependence of the pitch length on increasing the spacer

length from seven to eleven methylene units in a series of fluorinated dimers was reported by Saha *et al.* [89] and attributed to differences in the molecular bend angle between the two dimers in the N_{TB} phase. It has also been reported that changes in shape arising from inverting an ester linkage connecting the spacer to the mesogenic units in a dimer doubled the pitch length in the N_{TB} phase, although the molecular length was changed by a much smaller amount [90]. These changes also influence the bend elastic constant, K_{33} , to be discussed later, and this may contribute to the increase in pitch length on increasing spacer length.

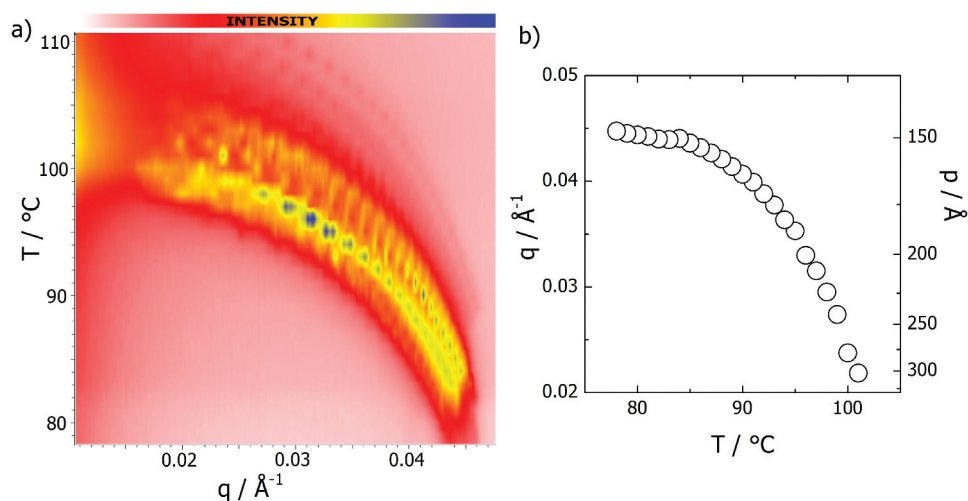


Figure 3. (Colour online) (a) Temperature evolution of the resonant soft X-ray diffraction signal in the N_{TB} phase measured on cooling and (b) the temperature dependence of the pitch length measured in the N_{TB} phase on cooling for CB15CB.

CB3CB melted directly into the isotropic liquid. On cooling, a strongly monotropic, reversible phase transition was observed at 47 °C. The texture associated with this phase appeared to consist of focal conic fans when viewed under the polarised optical microscope, in 3-micron cells treated for planar alignment, see Figure 4. The strongly monotropic nature of the phase precluded its study using X-ray diffraction. In order to assign this phase, a phase diagram was constructed using binary mixtures of CB3CB and the standard twist-bend nematogen, CB7CB [1], see Figure 5. Complete miscibility was observed over the entire range of compositions studied. The DSC traces obtained on cooling the mixtures are shown in Figure 6. For mixtures containing ≥ 70 mol % CB7CB, the phase sequence N_{TB} -N-I was observed. For the 80 and 90 mol % CB7CB mixtures, exotherms associated with each transition are observed, whereas for the 70 mol % mixture the nematic range is too short, and only a single broad exotherm is seen in the trace shown in Figure 6. Again, the N phase was identified on the basis of the observation of a characteristic schlieren texture, Figure 7(a), and the N_{TB} phase assigned by the

observation of a focal conic fan texture, Figure 7(b). As noted earlier, the N - N_{TB} phase transition was associated with the cessation of the optical flickering seen in the N phase. For the mixtures containing ≤ 60 mol % CB7CB, a direct N_{TB} -I transition was observed, and just a single exotherm is observed in the DSC traces, see Figure 6. The optical textures observed for the N_{TB} phase included both focal conic fan and polygonal textures, Figure 7(c,d) respectively. The focal conic fan texture arises from the pseudo-layered structure of the N_{TB} phase associated with the pitch length. The N -I phase transition temperature in the CB3CB:CB7CB phase diagram decreases linearly on increasing the mole fraction of CB3CB suggesting that the intermolecular energy parameter between the unlike species is the geometric mean of the interaction parameters between the like species [91]. This is an unsurprising result given the similar molecular structures of the two components. The line connecting the N_{TB} -N and N_{TB} -I transition temperatures also shows a linear dependence on increasing the concentration of CB3CB. The gradient of the N-I line is greater than that of the N_{TB} -N/I line, and these intercept at around 62 mol% CB7CB, see

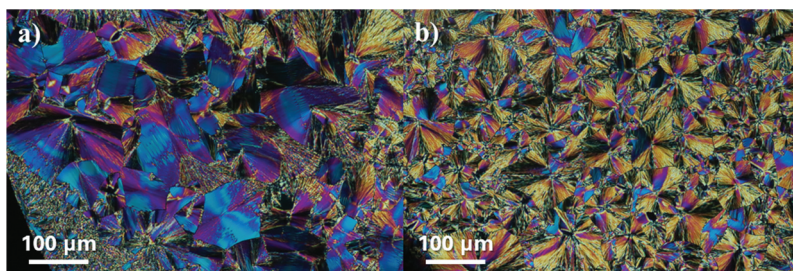


Figure 4. (Colour online) Optical textures observed on cooling CB3CB in a 3 μ m cell treated for planar alignment: (a) a focal conic fan texture with parabolic defects ($T = 47$ °C) and (b) a focal conic fan texture ($T = 46$ °C). These are examples of the natural textures of the N_{TB} phase.

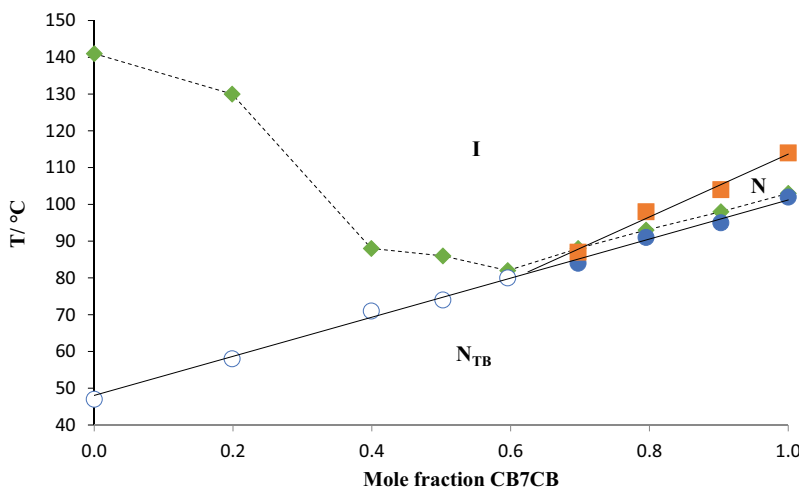


Figure 5. (Colour online) Phase diagram constructed for binary mixtures of CB3CB and CB7CB. Squares denote T_{NI} , filled circles $T_{N_{TB}N}$, open circles $T_{N_{TB}I}$ and diamonds the melting points.

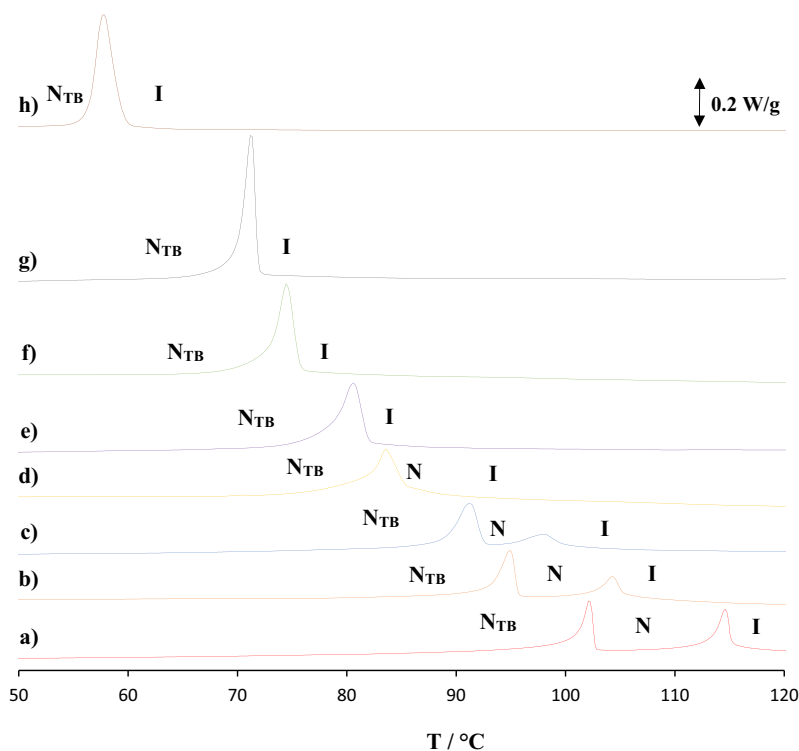


Figure 6. (Colour online) DSC traces obtained on cooling from the isotropic phase for (a) CB7CB and for the CB7CB:CB3CB mixtures (b) 90:10; (c) 80:20; (d) 70:30; (e) 60:40; (f) 50:50; (g) 40:60; (h) 20:80 mol %. The crystallisation exotherms are not shown.

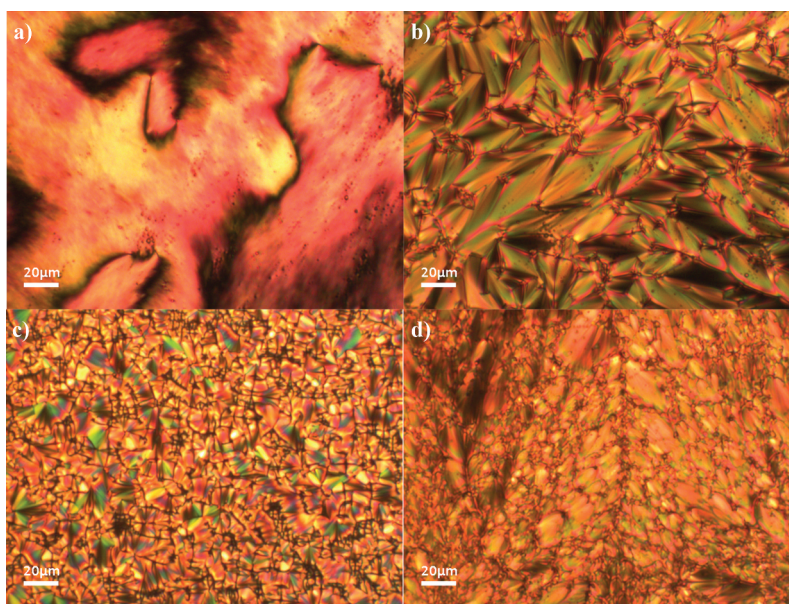


Figure 7. (Colour online) Optical textures observed for CB7CB:CB3CB mixtures: (a) schlieren texture of the N phase ($T = 101$ °C) and (b) focal conic texture of the N_{TB} phase ($T = 94$ °C) shown by the 90:10 mol % mixture; (c) focal conic texture of the N_{TB} phase ($T = 65$ °C) seen for the 60:40 mol % mixture; (d) focal conic texture of the N_{TB} phase ($T = 58$ °C) shown by the 20:80 mol % mixture.

Figure 5. Critically, the transition temperature measured for pure CB3CB lies on the N_{TB} -N/I line, indicating that the transition described earlier is indeed a direct N_{TB} -I transition and confirms that the textures shown

in **Figure 4** are examples of the natural textures of the N_{TB} phase for a pure compound. This is particularly noteworthy given that N_{TB} -I transitions in pure materials have been observed only rarely [7,8,13,70,92,93]. The

transitional behaviour reported here for CB3CB agrees well with that reported in the literature by Arakawa and co-workers who based their N_{TB} phase assignment solely on optical textures [70]. An earlier report of CB3CB overlooked the monotropic liquid crystalline behaviour reported here [69].

CB1CB also melted directly into the isotropic phase and on cooling, crystallised without showing any other liquid crystal phase behaviour. In order to determine a virtual I- N_{TB} transition temperature for CB1CB, a phase diagram was constructed using binary mixtures of CB1CB and CB7CB [1], see Figure 8. Miscibility was observed over the composition range for which liquid crystallinity was observed. The DSC traces obtained on cooling the mixtures that exhibited liquid crystallinity are shown in Figure 9. The mixtures containing ≥ 80 mol % CB7CB exhibited N_{TB} and N phases, whereas those containing ≤ 70 mol % CB7CB showed a direct N_{TB} -I transition. These transitions were identified using polarised light microscopy, see Figure 10, and included the observation of a rope-like texture, the formation of which was attributed to the undulation of pseudolayers during the temperature-induced shrinkage of the N_{TB} pitch [94,95]. As also seen in the CB3CB:CB7CB phase diagram (Figure 5), the N-I and N_{TB} -N/I lines both show a linear dependence on increasing the concentration of CB1CB, and the N-I line has the larger gradient, intersecting the N_{TB} -N line at around 70 mol % CB7CB (Figure 8). The CB1CB:CB7CB mixtures first show a direct N_{TB} -I transition at a lower concentration of CB1CB than seen for CB3CB in the mixtures of CB3CB:CB7CB. This presumably reflects the more bent structure of CB1CB. The mixtures containing ≤ 50 mol % CB7CB did not show liquid crystalline behaviour, and this may be attributed, at least in part, to the

sigmoidal dependence of the melting points of the mixtures on the concentration of CB1CB, and their dramatic increase below 60 mol % CB7CB (Figure 8). The virtual value of $T_{N_{TB}I}$ estimated for CB1CB is -3 °C although we note that this is obtained from a rather long extrapolation of the N_{TB} -N/I line and so must be treated with some degree of caution (Figure 8).

The dependence of the transition temperatures on the length of the flexible spacer for the odd members of the CB_nCB series is shown in Figure 11. The melting points decrease initially on increasing n before appearing to reach a limiting value. The first two odd members ($n = 1, 3$) show N_{TB} -I transitions, whereas CB5CB shows a narrow temperature range N phase in addition to the N_{TB} phase. The transition temperatures ($T_{N_{TB}N}$, $T_{N_{TB}N}$ or T_{NI}) increase sharply over the first three members of the series ($n = 1, 3, 5$). Further increasing n sees the values of both $T_{N_{TB}N}$ and T_{NI} pass through weak maxima for CB11CB, and begin to decrease, albeit very slowly. The temperature range of the N phase remains approximately constant for the higher values of n . We will return to a discussion of the trends in transition temperatures seen in Figure 10 later.

3.1.1. Refractive indices and birefringence

We now turn our attention to the material properties of these dimers. The temperature dependences of the extraordinary n_e and ordinary n_o refractive indices for CB13CB over the entire temperature range of the nematic phase are shown in Figure 12. Figure 13(a,b,c) presents the temperature dependencies of n_o for CB_nCB homologues $n = 7, 9, 11$ and 15, over the temperature range $0 \leq T - T_{NN_{TB}} \leq 6$ °C, for three different wavelengths. The ordinary refractive index n_o for all five dimers shows a very weak temperature dependence, in

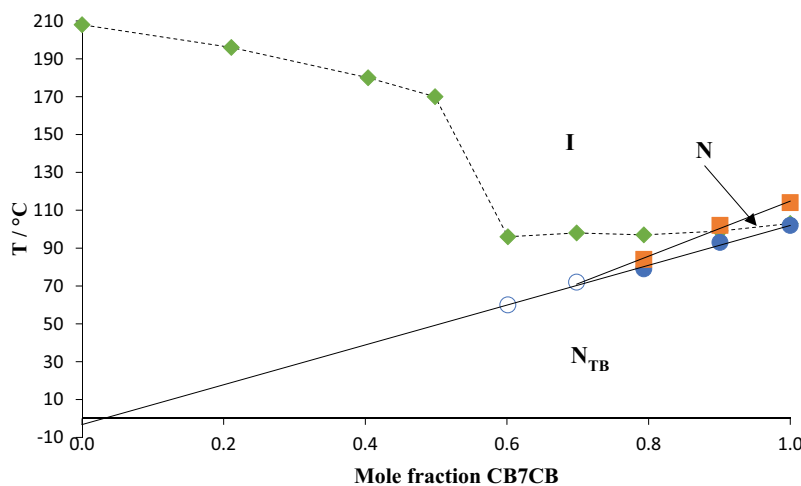


Figure 8. (Colour online) Phase diagram constructed for binary mixtures of CB1CB and CB7CB. Squares denote T_{NI} , filled circles $T_{N_{TB}N}$, open circles $T_{N_{TB}I}$ and diamonds the melting points.

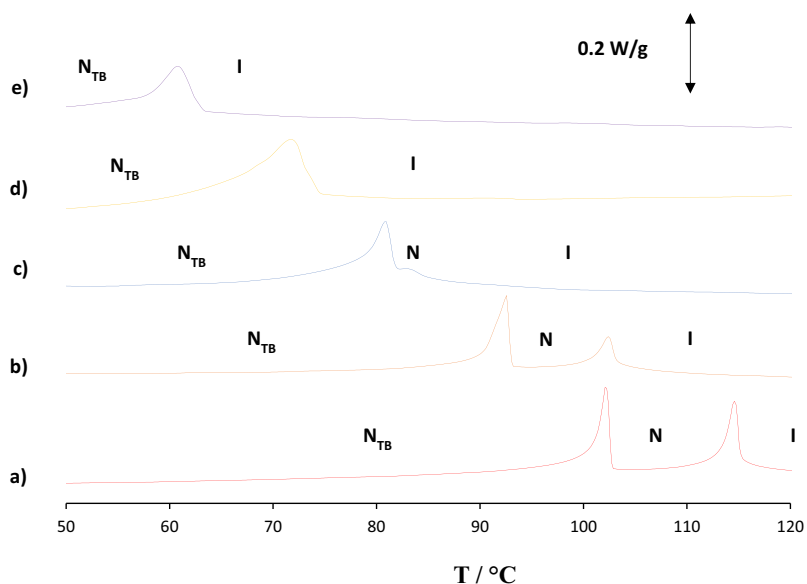


Figure 9. (Colour online) DSC traces obtained on cooling from the isotropic phase for (a) CB7CB and for the CB7CB:CB1CB mixtures (b) 90:10; (c) 80:20; (d) 70:30; (e) 60:40 mol %. The crystallisation exotherms are not shown.

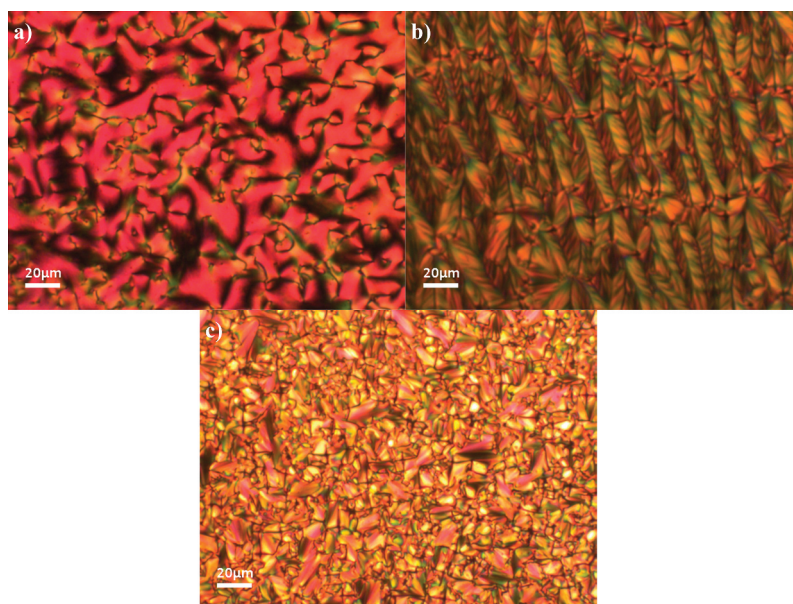


Figure 10. (Colour online) Optical textures observed for the CB7CB:CB1CB mixtures: (a) schlieren texture of the N phase ($T = 85\text{ }^{\circ}\text{C}$) and (b) rope-like texture of the N_{TB} phase with undulating pseudolayers ($T = 60\text{ }^{\circ}\text{C}$) shown by the 80:20 mol % mixture; (c) the natural focal conic fan texture of the N_{TB} phase obtained by cooling the isotropic phase ($T = 74\text{ }^{\circ}\text{C}$) for the 60:40 mol % mixture.

agreement with the previous measurements reported for CB7CB and CB11CB [64]. As the molecular length increases, n_o decreases, Figure 13(d,e,f); a similar trend has been reported for the cyanobiphenyl monomers by Sarkar *et al.* [96].

The temperature dependence of the birefringence, $\Delta n(T)$, for the N phase of the $CBnCB$ dimers, deduced from the measurements of optical retardance in flat planar cells, is shown in Figure 14. The measured value of $\Delta n(T)$ for CB13CB is consistent with the

wedge cell data, Figure 12. The birefringence $\Delta n(T)$ increases as n increases from 7 to 15, and this may be attributed to the higher optical polarisability of longer molecules [97]. A similar trend is seen for fluorinated dimers that also form the N_{TB} phase [98]. On the other hand, the trend is opposite to the behaviour observed in conventional monomeric cyanobiphenyls, in which the birefringence decreases in higher homologues with longer aliphatic terminal chains [96]. On cooling from the isotropic phase, $\Delta n(T)$ increases for all the dimers as

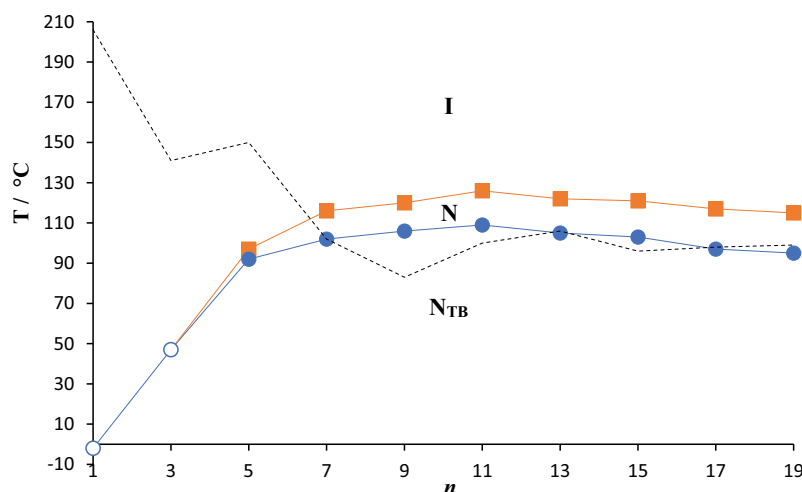


Figure 11. (Colour online) The dependence of the transition temperatures on the length of the alkyl spacer, n , for the odd members of the CB_nCB series. The squares denote T_{NI} , the empty circles T_{NTB} and the filled circles T_{NTB-N} . The broken line connects the melting points.

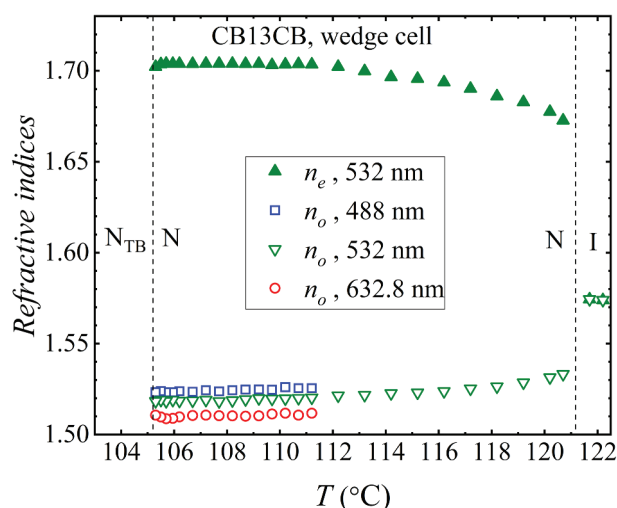


Figure 12. (Colour online) Temperature dependence of extraordinary refractive index n_e at 532 nm and ordinary refractive index n_o at 488 nm, 532 nm and 632.8 nm for CB13CB in a wedge cell.

the orientational order increases with decreasing temperature. As the temperature is reduced towards the $N-N_{TB}$ transition, $\Delta n(T)$ behaves differently in different homologues: (i) Δn increases for CB7CB, as reported by Meyer *et al.* [99], and CB9CB; (ii) Δn saturates for CB11CB; (iii) Δn slightly decreases for CB13CB and CB15CB. The pretransitional decrease of $\Delta n(T)$ close to the $N-N_{TB}$ transition is observed for other flexible dimers [2,98,100,101].

3.2. Dielectric anisotropy

The temperature dependencies of the dielectric permittivities measured when the electric field is parallel to the

director, $\epsilon_{\parallel}(T)$, and perpendicular to it, $\epsilon_{\perp}(T)$, are plotted in Figures 15(a–e). Figure 15(f) shows that ϵ_{\perp} decreases substantially as the molecular length increases, while ϵ_{\parallel} shows a much weaker dependence on n . As a result, the dielectric anisotropy $\Delta\epsilon(T)$, which is positive for all homologues, increases as the flexible alkyl spacer increases in length, Figure 16, similar to the behaviour seen for $\Delta n(T)$ in Figure 14. The same trend is observed for the absolute value of the negative $\Delta\epsilon(T)$ measured in fluorinated dimers [98]; however, conventional monomeric cyanobiphenyls show an opposite behaviour, as $\Delta\epsilon(T)$ decreases in homologues with longer aliphatic end chains [96]. As a function of temperature, $\Delta\epsilon(T)$ is weakly non-monotonous, decreasing as the temperature approaches the transition points to the isotropic phase and to the N_{TB} phase, Figure 16; the latter can be attributed to the formation of pretransitional clusters with twist-bend molecular arrangements.

3.3. Bend elastic constant, K_{33} , in the N^* phase

The transition temperatures of the CB_nCB dimers and their binary chiral mixtures with S811 (Figure 17(a)) are shown in Table 2. These temperatures have been measured on cooling and this accounts for the small differences observed in the transition temperatures for CB15CB compared to those listed in Table 1. The textures of the chiral mixture CB13CB:S811 in the cholesteric (N^*) and chiral twist bend nematic phase (N_{TB}^*) are shown in Figure 17(b) and (c), respectively.

The measurement of K_{33} in the Ch_{OH} state is based on the dependence of the peak Bragg reflection wavelength λ_p on the applied electric field E [64,77]. In this method,

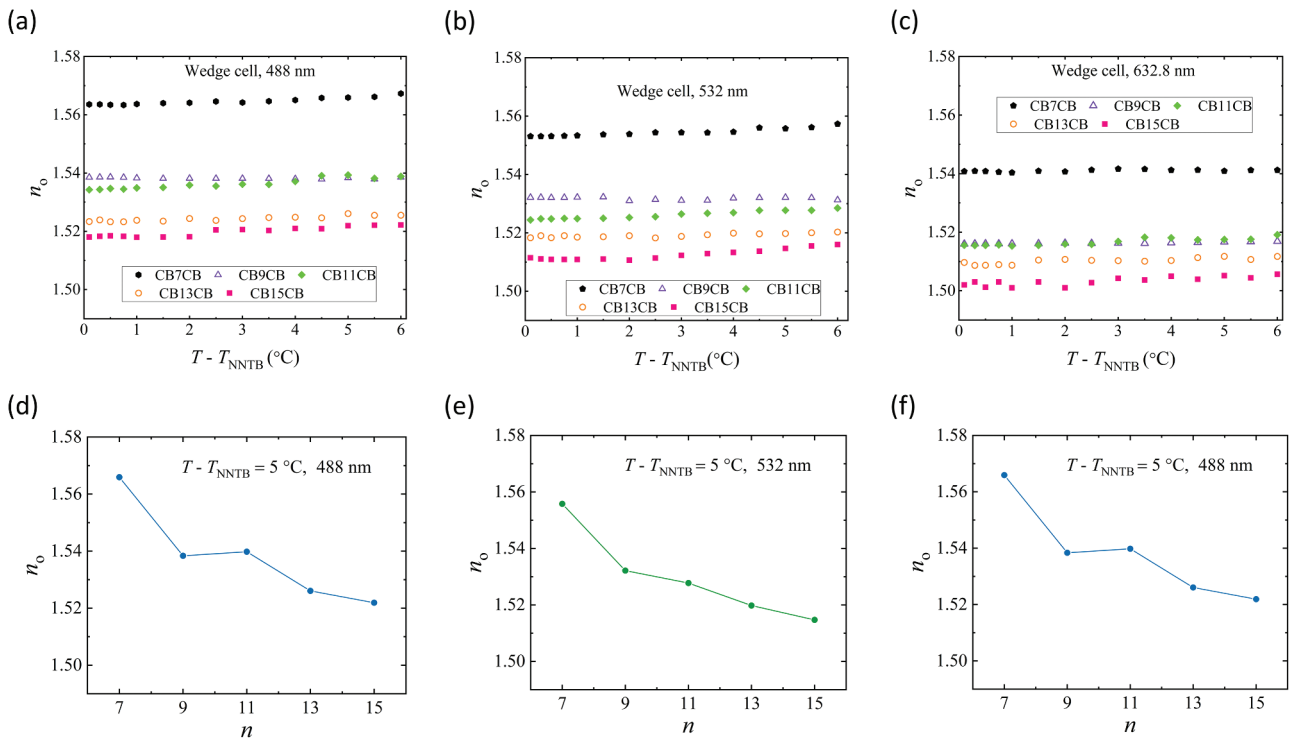


Figure 13. (Colour online) Temperature (a,b,c) and molecular length (d,e,f) dependencies of the ordinary refractive index n_o for $\text{CB}n\text{CB}$ dimers in the range $0 \leq T - T_{\text{NNTB}} \leq 6$ °C at wavelengths (a,d) 488 nm, (b,e) 532 nm and (c,f) 632.8 nm. The error bars are smaller than the size of the plot symbols. The reference transition temperatures are $T_{\text{NNTB}} = 102.2$ °C for $n = 7$, $T_{\text{NNTB}} = 106.4$ °C for $n = 9$, $T_{\text{NNTB}} = 107.9$ °C for $n = 11$, $T_{\text{NNTB}} = 105.2$ °C for $n = 13$ and $T_{\text{NNTB}} = 101.3$ °C for $n = 15$.

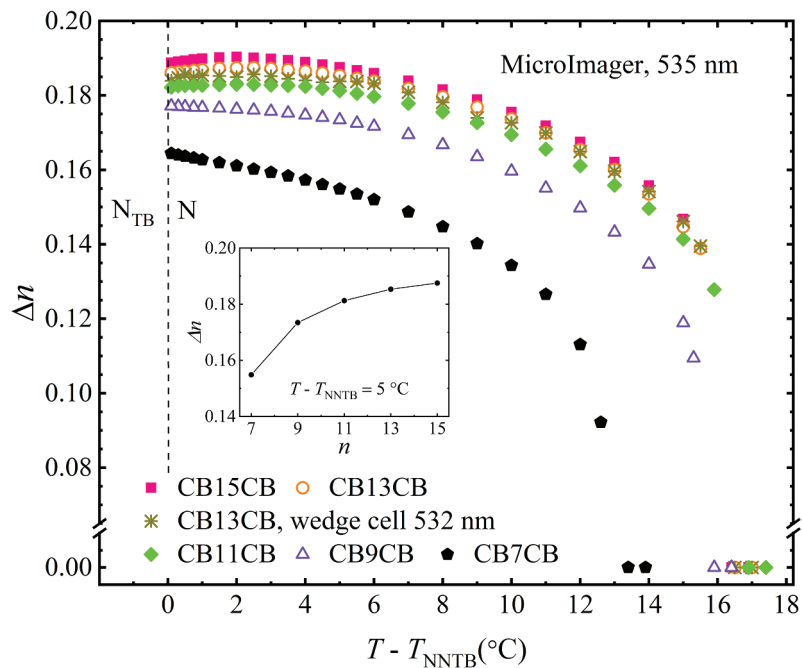


Figure 14. (Colour online) Temperature dependence of $\Delta n(T)$ for odd members of the $\text{CB}n\text{CB}$ series in the N phase measured at the wavelength 535 nm. The inset shows the dependence on the molecular length at a fixed temperature $T - T_{\text{NNTB}} = 5$ °C. The error bars are smaller than the size of the plot symbols.

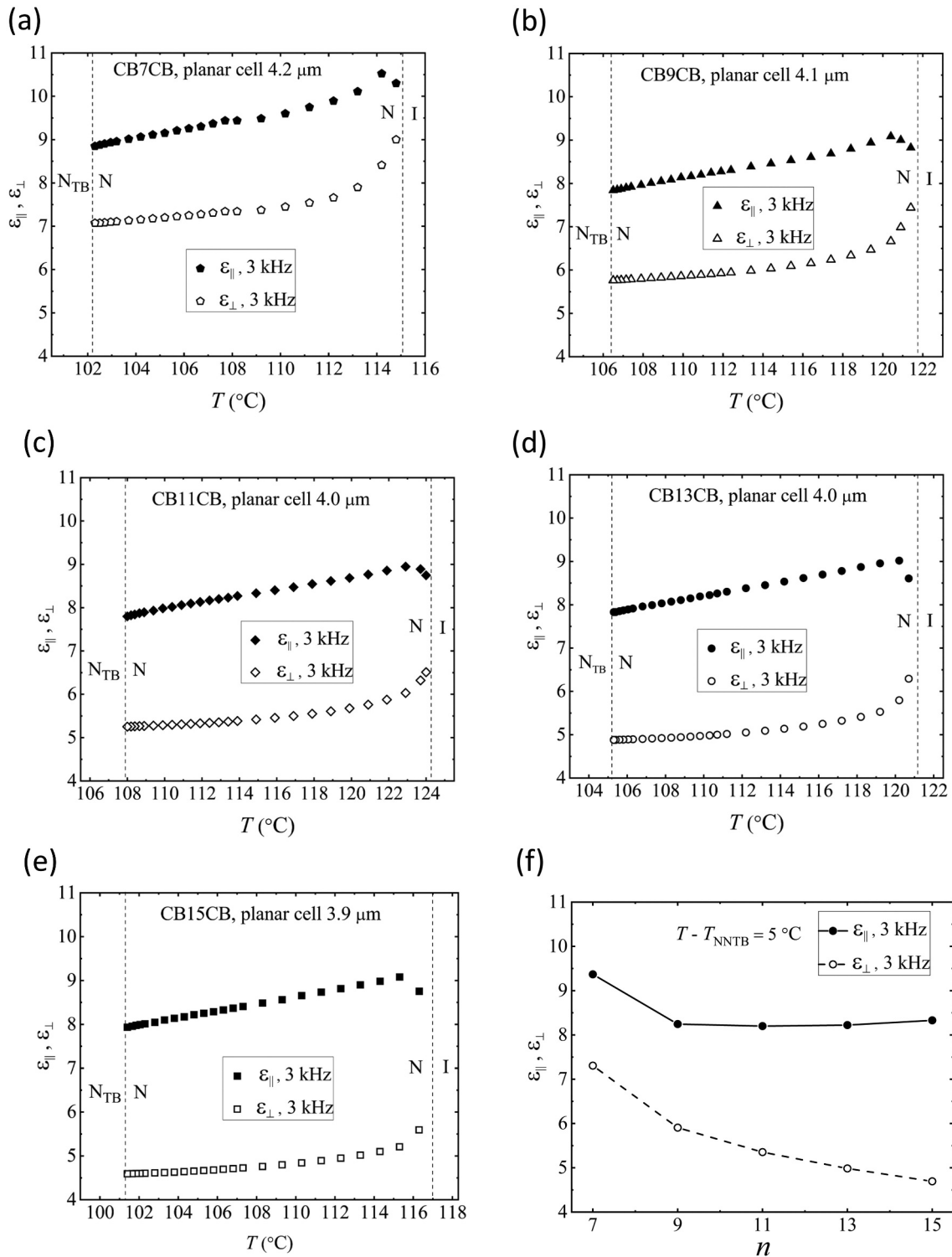


Figure 15. (a–e) temperature dependencies of dielectric permittivities of the nematic phase at 3 kHz for (a) CB7CB, (b) CB9CB, (c) CB11CB, (d) CB13CB and (e) CB15CB. (f) Dielectric permittivities as a function of the flexible spacer length at a fixed temperature $T - T_{\text{NNTB}} = 5$ °C.

the experimentally measured $\lambda_p/n_o(\lambda_p)$ is plotted against E^{-1} at each temperature point of interest. The dispersion of the ordinary refractive index $n_o(\lambda_p)$ is calculated using the Cauchy relation $n_o(\lambda) = A + B\lambda^{-2} + C\lambda^{-4}$, where the

coefficients A , B and C are determined using n_o values measured at three different wavelengths, Figure 13. The plot of $\lambda_p/n_o(\lambda_p)$ against E^{-1} is fitted with the polynomial $\alpha_1 E^{-1} + \alpha_2 E^{-2}$ to find the fitting parameters α_1 and α_2 ,

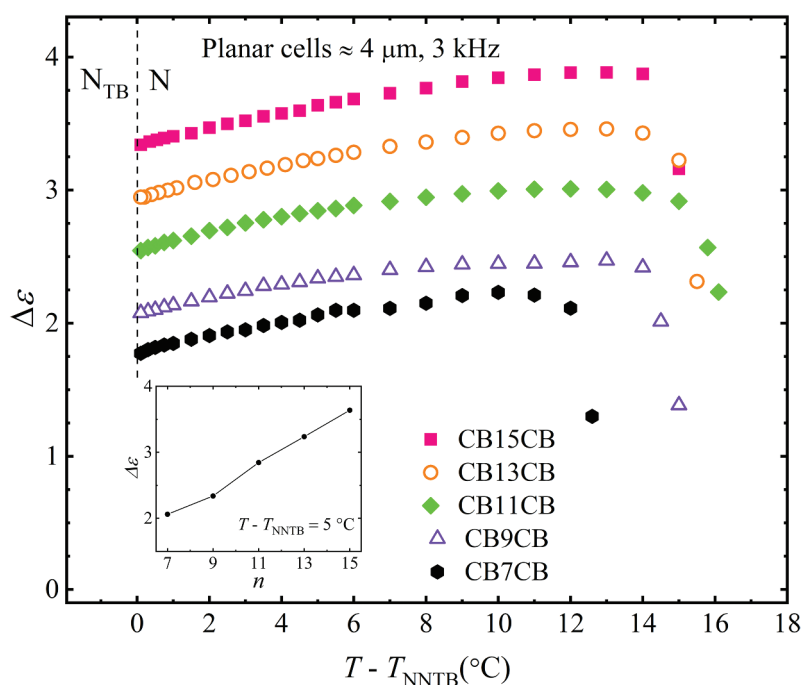


Figure 16. (Colour online) Temperature dependencies of dielectric anisotropy for CB_nCB dimers in the nematic phase at 3 kHz; the inset shows the variation with flexible spacer length n at a fixed temperature $T - T_{N_{NTB}} = 5$ °C.

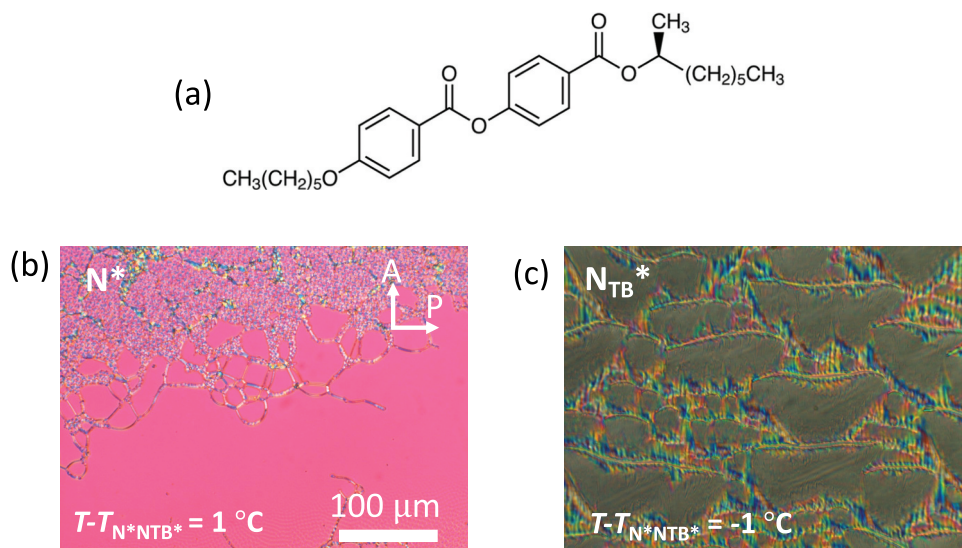


Figure 17. (Colour online) (a) Molecular structure of a chiral additive S811. Optical textures of CB13CB:S811 in a 20 μm planar cell showing (b) the N^* phase and (c) the N_{TB}^* phase, the chiral analogue of the N_{TB} phase. The optical textures are taken using a polarising optical microscope Nikon OPTIPHOT2-POL equipped with an objective: M plan $\times 20$, N.A. 0.40, ELWD and condenser: N.A. 0.1, LWD (Nikon Instruments Inc.).

where the correction $\alpha_2 E^{-2}$ turns out to be negligibly small compared to $\alpha_1 E^{-1}$. The obtained value of α_1 is used to evaluate $K_{33} = \epsilon_0 \Delta\epsilon (\alpha_1)^2 / 4\pi^2$. The dielectric anisotropy $\Delta\epsilon(T)$ at the temperatures of interest is measured in the N phase of the corresponding chiral mixtures as described earlier.

The measured temperature dependence $K_{33}(T)$ is non-monotonous in all CB_nCB :S811 (96:4 wt.%) chiral mixtures, **Figure 18**. $K_{33}(T)$ decreases essentially linearly on cooling the N_{TBI} phase, passes through a minimum value at approximately $T - T_{N^*NTB^*} = 1$ °C and subsequently increases near the transition to the

Table 2. Transition temperatures of the CB n CB dimers and the CB n CB:S811 (96:4 wt.%) chiral mixtures measured on cooling from the isotropic phase.

Compound	$T_{IN}^*/^{\circ}C$	$T_{N_{TB}N}^*/^{\circ}C$	Chiral mixture	$T_{IN}^*/^{\circ}C$	$T_{N^*N_{TB}^*}^*/^{\circ}C$
CB7CB	115.1	102.2	CB7CB:S811	107.0	94.1
CB9CB	121.8	106.4	CB9CB:S811	111.7	96.3
CB11CB	124.3	107.9	CB11CB:S811	116.5	100.3
CB13CB	121.2	105.2	CB13CB:S811	114.3	98.3
CB15CB	117.2	101.3	CB15CB:S811	113.7	97.8

N_{TB}^* phase. Similar behaviour has been reported for other odd-membered dimers [102]. This behaviour becomes more pronounced in higher homologues. For CB7CB:S811(96:4 wt.%), $K_{33}(T)$ in Figure 18 is very close to $K_{33}(T)$ reported previously for the N phase of pure CB7CB [73], and for the same CB7CB:S811 (96:4 wt.%) chiral mixture in the Ch_{OH} state [64]. Furthermore, $K_{33}(T)$ of the CB11CB:S811 (96:4 wt.%) mixture is similar to the data for a CB11CB:S811 (97:3 wt.%) mixture [64]. The minimum of $K_{33}(T)$ becomes deeper as n increases from 7 to 15, which reflects the higher flexibility of longer spacers, see inset in Figure 18. The lowest value of $K_{33} = 0.05$ pN in $n = 15$, is slightly smaller than the measured 0.065 pN in chiral mixtures CB7CB:CB11CB:5CB = 52:31:17 (wt.%) with 1.8 wt.% and 4.2 wt.% of S811 [64]. We note that the reflection spectra are hard to detect in the vicinity of the $N^*-N_{TB}^*$ transition; in the CB7CB:S811, CB9CB:S811 and CB11CB:

S811 mixtures, the reflection spectra are observed at $T \geq T_{N^*N_{TB}^*} + 0.1$ °C; in CB13CB:S811, at $T \geq T_{N^*N_{TB}^*} + 0.2$ °C, and in CB15CB:S811, at $T \geq T_{N^*N_{TB}^*} + 0.35$ °C. The disappearance of the Bragg reflection in the pre-transitional region may be associated with the destruction of the Ch_{OH} state by pretransitional cybotactic groups of the N_{TB}^* phase; the equidistance of the pseudolayers of the N_{TB}^* clusters yields a higher value of K_{33} and prohibits the formation of the Ch_{OH} phase.

3.4. Molecular shape

We have already noted that it is widely accepted that the twist-bend nematic – nematic/isotropic transitions are predominantly shape driven. Indeed, a generalised Maier-Saupe molecular field theory developed to describe the phase behaviour of rigid V-shaped molecules revealed how sensitive the phase behaviour of such a system is to the molecular bend angle [103]. Specifically, as the bend

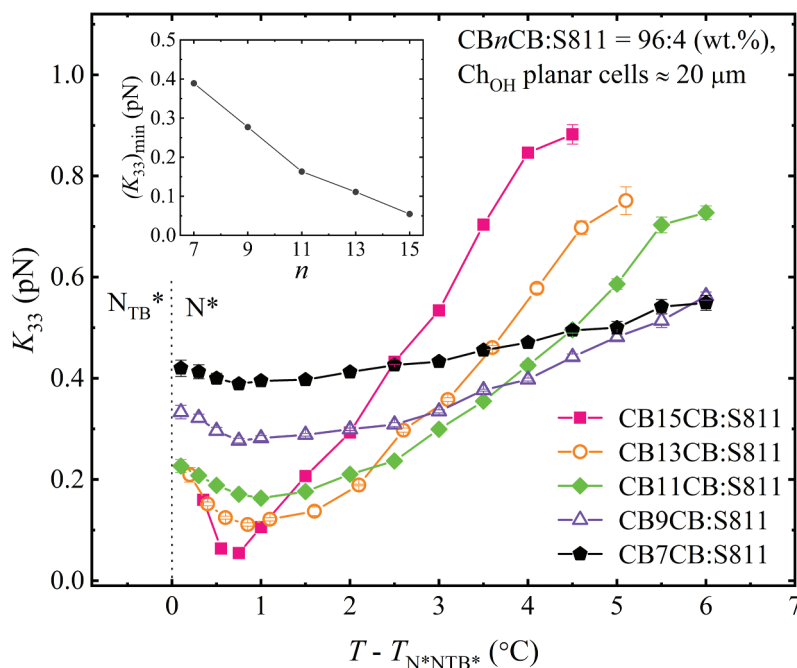


Figure 18. (Colour online) Temperature dependencies of the bend elastic constants $K_{33}(T)$ for the CB n CB:S811 chiral mixtures in the Ch_{OH} state. The inset shows the decrease of the minimum value of $K_{33}(T)$ with the flexible spacer length n . The reference transition temperatures are $T_{N^*N_{TB}^*} = 97.8$ °C for $n = 15$, $T_{N^*N_{TB}^*} = 98.3$ °C for $n = 13$, $T_{N^*N_{TB}^*} = 100.3$ °C for $n = 11$, $T_{N^*N_{TB}^*} = 96.3$ °C for $n = 9$ and $T_{N^*N_{TB}^*} = 94.1$ °C for $n = 7$.

angle becomes smaller, the temperature range of nematic behaviour is reduced and the N_{TB} phase becomes stabilised, and for bend angles $\leq 130^\circ$ an N_{TB} -I transition is predicted. By contrast, for bend angles $\geq 150^\circ$, the N_{TB} -N transition temperature is predicted to occur only at very low temperatures. Thus, to understand the dependence of the phase transition temperatures on the spacer length, n , shown in Figure 11, we must first consider how increasing n changes the molecular shape. Figure 19 compares the molecular shapes of the all-*trans* conformations of short, intermediate, and long members of the $CBnCB$ series. $CB1CB$ has a rather different shape and flexibility to the other members of the series and may be described by a molecular bend angle of 116.0° defined by the $C_{Ar}-C-C_{Ar}$ bond angle at the centre of the molecule. The question now arises as to how to best capture the difference in molecular shape as n increases. The most common approach to describe the bend of an odd-membered dimer is to use the angle subtended by the two nitrile bonds, given as angle Y in Figure 20, but this does not, in fact, differentiate between spacer lengths. Instead, the angle remains constant at approximately 113° , but the intersection of the lines falls progressively below the molecule as n increases, see Figure 20. It is quite apparent that the shapes of these molecules ($n \geq 3$) may be described as isosceles trapezoids, and a possible means of capturing the molecular bend of such a structure is to use the angle Z shown in Figure 20. The calculation of this angle is described in the ESI, and the values of this angle for the $CBnCB$ series are listed in Table 3. It is clear that the molecular bend angle defined in this way increases as n increases, and it may, at first sight, appear counter-intuitive that the stability of the N_{TB} phase increases sharply as the bend angle increases over the first three members, see Figure 11. We must remember, however, that the flexibility of the molecule also increases on increasing n , and this facilitates the better interaction between the mesogenic groups. These interactions compensate for the loss of entropy due to the additional polar order in the N_{TB} phase [103], counteracting the effect of the increasing bend angle, and the stability of the N_{TB}

phase increases. These interactions between the mesogenic units will also promote the emergence of the N phase. Thus, on increasing n we see initially an increase in the stability of both the N_{TB} and N phases. At some point, the N phase will become more stable, and for the $CBnCB$ series, this occurs for $n = 5$. Further increasing n will continue to promote both the N and N_{TB} phases through the enhanced interactions between the mesogenic units, whereas the increasing bend angle presumably destabilises the N_{TB} phase. Increasing n still further dilutes the interactions between the mesogenic units as the volume fraction of alkyl chain increases, and both T_{NI} and $T_{N_{TB}N}$ would be expected to pass through maximum values and begin to decrease. For the $CBnCB$ series, this occurs for $n = 11$. As we have seen, however, the minimum value of $K_{33}(T)$ decreases monotonically on increasing spacer length reflecting the increased flexibility and this will drive the elastic instability related to the formation of the N_{TB} phase counteracting, at least in part, the expected decrease in $T_{N_{TB}N}$ related to the dilution of the mesogenic units. This interpretation accounts for the behaviour seen in Figure 11. We do note, however, that this is a simplified view of shape which has not taken into account the inherent flexibility of the spacer and a more realistic interpretation would necessarily consider a conformational distribution. Indeed, the very similar transition temperatures for the longer homologues

Table 3. Molecular bend angles for the $CBnCB$ and CBO_nOCB series as defined in Figure 20.

$CBnCB$	Bend angle/ $^\circ$	CBO_nOCB	Bend angle/ $^\circ$
1	116.0 [‡]	–	–
3	117.6	1	144.8
5	123.0	3	150.3
7	127.9	5	152.7
9	131.9	7	154.5
11	135.3	9	156.0
13	138.3	11	157.3
15	140.9	–	–
17	143.1	–	–
19	145.1	–	–

[‡]The $C_{Ar}-C-C_{Ar}$ bond angle.

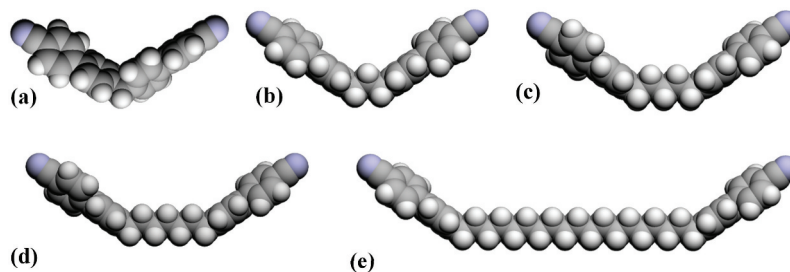


Figure 19. (Colour online) Space filling models comparing the all-*trans* molecular shapes of (a) $CB1CB$, (b) $CB3CB$, (c) $CB5CB$, (d) $CB7CB$ and (e) $CB19CB$.

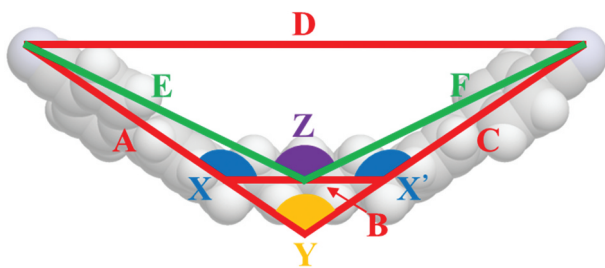


Figure 20. (Colour online) A space filling model of CB7CB showing the angle subtended by the two nitrile bonds falls below the molecule, Y , and the bend angle defined assuming the molecular shape is an isosceles trapezoid, Z .

presumably imply that their average molecular shapes are very similar.

3.5. CBO n OCB series

In order to investigate the effect of the bond angle, associated with the linking unit between the spacer and mesogenic units, on the transitional properties of the dimers, we revisited the CBO n OCB series and established values of $T_{N_{TB}N}$ for $n = 1, 7, 9$ and 11 , see Table 4. These complement our previous report of the values for 3 and 5 [67]. For $n = 7, 9$ and 11 , the N_{TB} phase was

identified on the basis of the observation of characteristic optical textures in isolated droplets when viewed under the polarised light microscope. These observations required extensive supercooling but the measured values are in excellent agreement with those reported recently by Arakawa and colleagues [34]. For CBO1OCB, the measured value of T_{NI} listed in Table 4 is somewhat higher than that reported previously whereas those for $n = 7, 9$ and 11 show excellent agreement [71,72]. In order to estimate a virtual value of $T_{N_{TB}N}$ for CBO1OCB, a phase diagram was constructed for binary mixtures of CBO1OCB and CB7CB, see Figure 21. Mixtures containing ≥ 40 mol % CB7CB exhibited N_{TB} and N phases. The N - I transition temperatures showed a linear dependence on the concentration of CBO1OCB, and the experimentally measured value of T_{NI} for isolated droplets of CBO1OCB fell exactly on this line confirming the assignment. The N_{TB} - N line also showed a linear dependence on concentration and extrapolation gave a virtual $T_{N_{TB}N}$ of 33 °C. We note, however, that this estimate required a long extrapolation of the N_{TB} - N line and so the value obtained must be treated with some degree of caution. Full details of these measurements are provided in the Supplementary Information along with representative textures from the mixtures as shown in Figure SI2.

Table 4. Transition temperatures and associated entropy changes for selected odd members of the CBO n OCB series.

n	$T_{Cr}/^{\circ}\text{C}$	$T_{N_{TB}N}/^{\circ}\text{C}$	$T_{NI}/^{\circ}\text{C}$	$\Delta S_{Cr}/R$	$\Delta S_{NI}/R$
1	149	33 ^a	104 ^b	10.8	–
7	138	85 ^b	181	17.3	0.83
9	135	81 ^b	172	14.7	1.03
11	125	78 ^b	164	12.9	1.04

^aVirtual transition temperature estimated from binary phase diagram with CB7CB. ^bMeasured using the polarised light microscope.

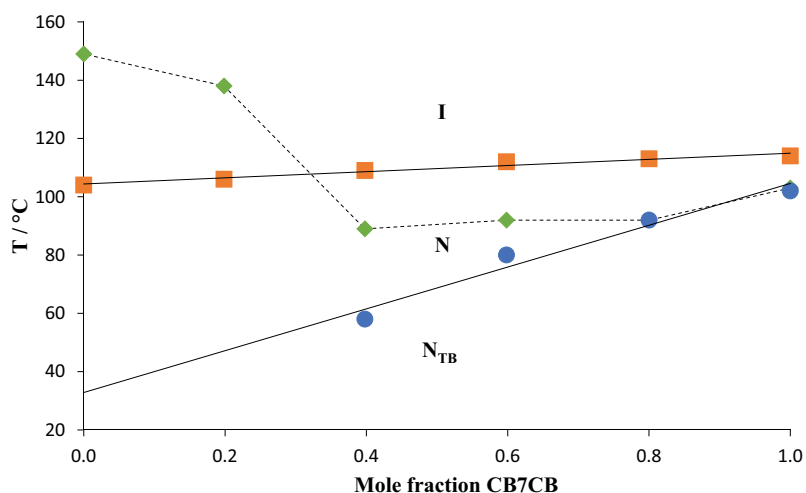


Figure 21. (Colour online) Phase diagram constructed for binary mixtures of CBO1OCB and CB7CB. Squares denote T_{NI} , circles $T_{N_{TB}N}$ and diamonds the melting points.

3.6. A comparison of the CB n CB and CBO n OCB series

The transition temperatures of the CB n CB and CBO n OCB series are compared in Figure 22. To make this a meaningful comparison, members of the two series having the same number of atoms connecting the two cyanobiphenyl units must be compared, and so the temperatures are plotted against p , where $p = n$ for the CB n CB series and $p = n + 2$ for the CBO n OCB series. The values of T_{NI} for the even members of both series decrease as p increases, and those of the CBO n OCB series are higher by, on average, 24 K. By contrast, the values of T_{NI} for the odd members of both series initially increase on increasing p , pass through a weak maximum and subsequently gradually decrease. The values of T_{NI} are again higher for the CBO n OCB series, and for the odd members, this difference between the two series is greater. For example, T_{NI} for CBO5OCB is some 73 K higher than that of CB7CB. As p increases, this difference in T_{NI} becomes smaller and reaches a limiting value of around 32 K. The combined effect of these trends is that the values of T_{NI} show a large odd-even effect for both series in which the even members show the higher values, and the magnitude of the alternation is greater for the CB n CB series. Similar experimental observations have been made when comparing other methylene- and ether-linked dimers [104,105], and these are in complete agreement with predictions of a theoretical model developed by Luckhurst and co-workers [106–108]. In this model, the only difference between the dimers is their shape, and this difference arises from the bond angle between the *para* axis of the mesogenic unit and the first bond in the spacer. For an ether link, this bond angle is 126.4° and for a methylene

link it is considerably smaller, 113.5°. For an even-membered dimer, this difference in angle does not change the angle subtended by the major axes of the two mesogenic units but does increase the molecular breadth giving rise to a reduction in T_{NI} , see Figure 23. By comparison, the smaller bond angle associated with the methylene link means that an odd-membered methylene-linked dimer is significantly more bent than its even-membered counterpart and this leads to a larger reduction in T_{NI} , see Figure 23. The overall effect, therefore, is that the values of T_{NI} for the methylene-linked dimer series show a more pronounced alternation than those of the corresponding ether-linked series. In addition, it is important to note that these alternations in T_{NI} attenuate on increasing p for both series such that for the longer spacers, odd and even membered dimers show essentially the same value of T_{NI} . This attenuation may be accounted for in terms of the increasing number of conformations available to the spacer and torsional fluctuations which results in a loss of orientational correlations between the mesogenic units. In addition to these shape-based arguments, we should also note that the strength of the interactions between cyanobiphenyloxy units will be greater than those between the cyanobiphenyl units, and this contributes to the higher values of T_{NI} seen for both the odd and even members of the CBO n OCB series.

We now turn our attention to the tendency of these two series to exhibit the N_{TB} phase. We have seen that CB1CB exhibits a virtual N_{TB}-I transition at -3 °C, whereas for CB3CB the N_{TB}-I transition is experimentally observed at 47 °C. By comparison, for CBO1OCB a virtual value of $T_{\text{N}_{\text{TB}}\text{N}}$ was estimated at 33 °C, and experimentally T_{NI} observed at 104 °C. Presumably, this

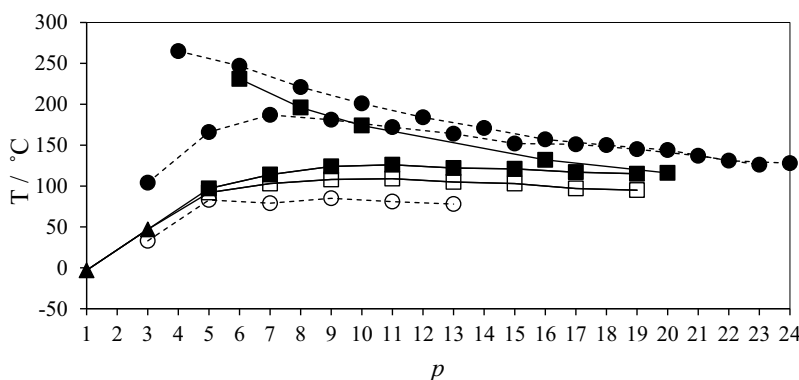


Figure 22. The dependence of the transition temperatures on the number of atoms, p , connecting the mesogenic units in the CB n CB and CBO n OCB series; for the CB n CB series $p = n$, and for the CBO n OCB series, $p = n + 2$. Filled circles represent N-I and open circles N_{TB}-N transitions for the CBO n OCB series. Filled squares represent N-I, open squares N_{TB}-N transitions and filled triangles N_{TB}-I transitions for the CB n CB series. Solid lines connect data points for the CB n CB series and the broken lines for the CBO n OCB series. The data have been taken from a number of sources [67,71,72]. The transition temperatures of the CBO n OCB series ($n \geq 13$) were reported prior to the discovery of the N_{TB} phase and these have not been revisited [71].

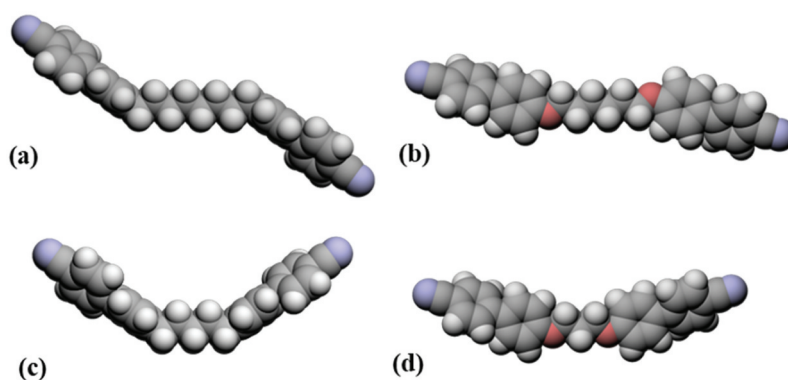


Figure 23. (Colour online) Space filling models comparing the all-*trans* molecular shapes of (a) CB8CB, (b) CBO6OCB, (c) CB5CB and (d) CBO3OCB, highlighting the effect of changing the linking unit between the spacer and mesogenic units.

difference in behaviour reflects the more bent shape of CB3CB arising from the methylene links, see Figure 19, and the greater ability of the mesogenic units in CBO1OCB to interact. Over the shortest odd members, the values of $T_{N_{TB}N}$ or $T_{N_{TB}N}$ increase sharply. For $p = 5$, the value of $T_{N_{TB}N}$ for CB5CB is 9 K higher than that of CBO3OCB, although T_{NI} for the latter is 69 K higher than that of CB5CB. After $p = 5$, the dependence of $T_{N_{TB}N}$ on p for both series becomes rather weak, and the values of $T_{N_{TB}N}$ for the CB n CB series are on average 25 K higher. By contrast, a stronger dependence is observed for the values of T_{NI} which increase by 8 K between $p = 7$ and 13 for the CB n CB series but decrease for the CBO n OCB series by 31 K. As noted earlier, increasing the spacer length in these odd-membered dimers increases the ability of the mesogenic units to interact but also dilutes these interactions. For the N-I transition, the latter effect appears to dominate for the CBO n OCB series and the former for the CB n CB series reflecting the more bent shape of the methylene-linked dimers, see Table 3. The less sensitive nature of $T_{N_{TB}N}$ on p presumably reflects its stronger dependence on shape and hence, as discussed earlier, on K_{33} . For the odd-membered dimers with $p = 7-13$, the CB n CB series shows a larger change in the bend angle but presumably this is offset by the greater ability of the mesogenic units to interact as the bend angle increases giving little overall change in the value of $T_{N_{TB}N}$ as spacer length increases.

3.7. CB16CB and CB20CB

The transitional properties of the two new long even-members of the CB n CB series, CB16CB and CB20CB, are also listed in Table 1. Both dimers exhibit enantiotropic nematic behaviour and no other liquid crystalline phase. As described earlier, the values of T_{NI} for the even members of the CB n CB series decrease on increasing n , whereas those of the odd members initially increase with n , pass through a maximum and tend towards a limiting value, Figure 22. The value of T_{NI} for CB20CB is essentially the same as that of the adjacent odd members, suggesting that their average molecular shapes are similar. Figure 24 shows the all-*trans* molecular shapes for CB16CB and CB17CB. In the even-membered dimer, the mesogenic units are parallel whereas the odd member adopts the trapezium shape discussed earlier. Presumably, the conformational flexibility of these long spacers allows the mesogenic units in the odd and even members to interact to much the same extent and may suggest that their average molecular shapes are similar. This begs the fascinating question, can long even-membered dimers exhibit the N_{TB} phase? To explore this intriguing possibility, phase diagrams were constructed for binary mixtures of each dimer with CB7CB, see Figure 25. In both phase diagrams, T_{NI} varies in a linear fashion with composition as might be expected given their very similar molecular structures. Increasing the concentration of the even-membered dimer in the mixture sees the value of $T_{N_{TB}N}$ fall rapidly, and the N_{TB} phase is not observed in either system for mixtures containing

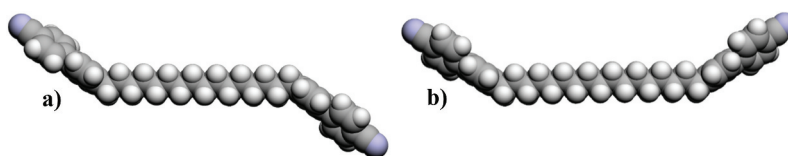


Figure 24. (Colour online) Space filling models comparing the all-*trans* molecular shapes of (a) CB16CB and (b) CB17CB.

≤ 70 mol % CB7CB. The virtual value of $T_{N_{TB}N}$ for the even membered dimers may be estimated by extrapolation of the $T_{N_{TB}N}$ line, although it is stressed that the extrapolation is rather long in both cases. The estimated values of $T_{N_{TB}N}$ for CB16CB and CB20CB are -13 °C and 1 °C, respectively, and around 100 K lower than seen for the adjacent odd members. This strongly suggests that, on average, the long odd-membered dimers are more bent than their even-membered counterparts, and the similarity in their values of T_{NI} may be attributed to the increased ease at which the mesogenic units in odd-membered dimers can interact on increasing the spacer length.

4. Conclusions

We have reported the transitional properties of the CB_nCB series, the most complete set of odd-membered dimers to date. This has revealed that the shortest members show

direct N_{TB} -I transitions and as spacer length increases, we see the N_{TB} -N-I sequence. These observations and a comparison of the transitional properties of the CB_nCB and $CBOnOCB$ series have reinforced the importance of shape in the formation of the N_{TB} phase. This is attributed to the dependence of material properties such as dielectric permittivities, refractive indices and bend elastic constant on molecular shape. A longer flexible spacer yields higher birefringence and dielectric anisotropy. The temperature dependence of the bend modulus is non-monotonous, with a pronounced minimum at about 1 °C above the transition point to the twist-bend phase; the minimum is deeper for longer homologues, with CB15CB doped with a chiral S811 showing the lowest bend elastic constant (0.05 pN) in any liquid crystal measured so far. In an attempt to capture the shape of these symmetric dimers, we have suggested that they are approximated to an isosceles trapezium. This approach reveals a bend angle which increases as the spacer length increases, effectively resulting

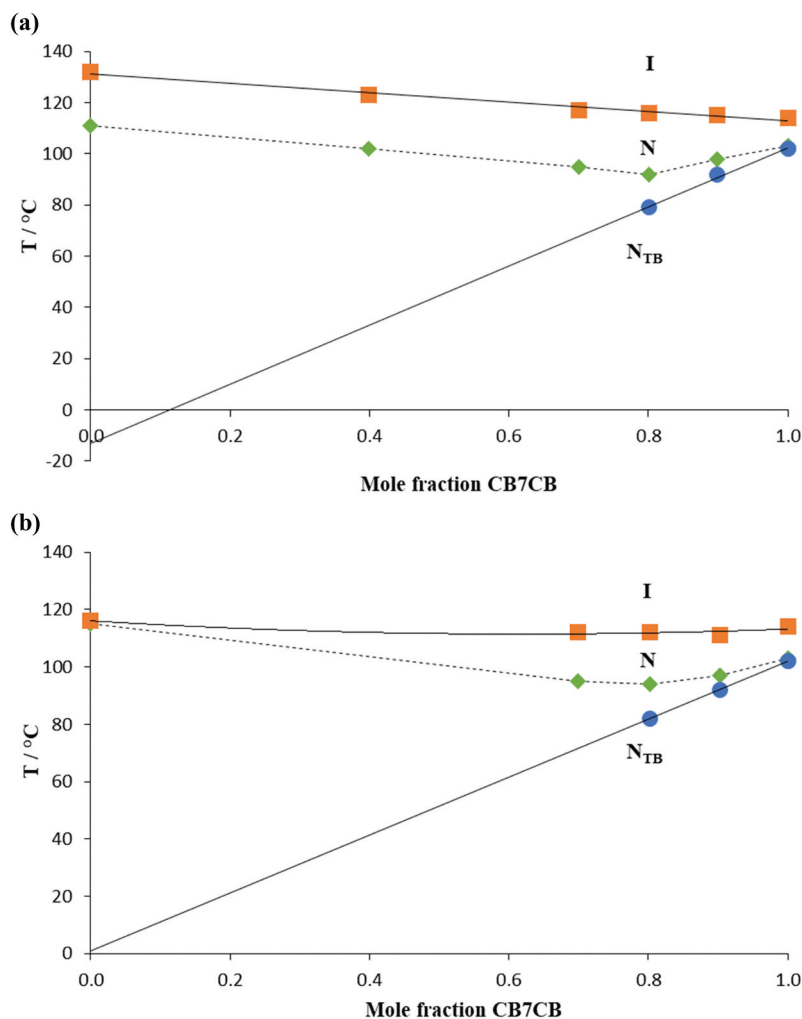


Figure 25. (Colour online) Phase diagrams constructed using binary mixtures of (a) CB16CB and CB7CB, and (b) CB20CB and CB7CB. The squares indicate N-I transitions, the circles N_{TB} -N transitions and the diamonds melting points. The solid lines indicate the T_{NI} and $T_{N_{TB}N}$ trends, and the dotted line connects the melting points.

in longer and more linear molecular shapes. These shape changes might explain the increase of the birefringence and dielectric anisotropy with n , a behaviour clearly at odds with the previously reported dependencies on the length of aliphatic terminal chains in homologous series of cyanobiphenyls and similar nematic mesogens [96]. Although it is apparent that the N_{TB} -N phase transition is predominantly shape driven, it is not entirely so. This is clear when comparing the values of $T_{N_{TB}N}$ for the $CBnCB$ and CBO_nOCB series. As would be expected, the values of T_{NI} for the CBO_nOCB series are much higher than those of the corresponding members of the $CBnCB$ series. By comparison, their values of $T_{N_{TB}N}$ are rather similar and this appears counter-intuitive if considering shape alone. It is clear that the interaction strength between the mesogenic units also plays a role in determining $T_{N_{TB}N}$. Thus, although the odd members of the $CBnCB$ series are clearly more bent than the corresponding CBO_nOCB dimers, the stronger interactions between the cyanobiphenyloxy units ensure that the values of $T_{N_{TB}N}$ for the longer members of the series are surprisingly similar. These stronger interactions are manifested to a much greater extent in much higher values of T_{NI} for the CBO_nOCB series. We have reported also that whereas long even-membered and odd-membered dimers show very similar values of T_{NI} , the former do not exhibit N_{TB} behaviour. This is attributed to the ability of the mesogenic units in these dimers to interact essentially the same irrespective of the parity of the spacer but the odd members retain their more bent shape. Thus, the transitional behaviour of dimers may be interpreted in terms of the molecular bend angle, the ability of the mesogenic units to interact and the diluting factor of the spacer chain.

Acknowledgments

The RSoXS experiments were performed at beamline 11.0.1.2 at the Advanced Light Source at the Lawrence Berkeley National Laboratory, supported by the Director of the Office of Science, Office of Basic Energy Sciences, of the U.S. Department of Energy under Contract No. DE-AC02-05CH11231. ODL and KT research was supported by the US National Science Foundation grant DMR-2215191.

Disclosure statement

No potential conflict of interest was reported by the author(s).

Funding

The work was supported by the National Science Foundation [DMR-2215191]; U.S. Department of Energy [DE-AC02-05CH11231].

ORCID

Ewan Cruickshank  <http://orcid.org/0000-0002-4670-8405>

Oleg Lavrentovich  <http://orcid.org/0000-0002-0128-0708>

Corrie T Imrie  <http://orcid.org/0000-0001-6497-5243>

References

- [1] Cestari M, Diez-Berart S, Dunmur DA, et al. Phase behavior and properties of the liquid-crystal dimer 1',7''-bis(4-cyanobiphenyl-4'-yl) heptane: a twist-bend nematic liquid crystal. *Phys Rev E*. 2011;84(3):031704. doi: [10.1103/PhysRevE.84.031704](https://doi.org/10.1103/PhysRevE.84.031704)
- [2] Borshch V, Kim YK, Xiang J, et al. Nematic twist-bend phase with nanoscale modulation of molecular orientation. *Nat Commun*. 2013;4(1):2635. doi: [10.1038/ncomms3635](https://doi.org/10.1038/ncomms3635)
- [3] Chen D, Porada JH, Hooper JB, et al. Chiral heliconical ground state of nanoscale pitch in a nematic liquid crystal of achiral molecular dimers. *Proc Natl Acad Sci USA*. 2013;110(40):15931–15936. doi: [10.1073/pnas.1314654110](https://doi.org/10.1073/pnas.1314654110)
- [4] Meyer RB. Structural problems in liquid crystal physics, les houches summer school in theoretical physics. In: Balian R W G, editors. *Molecular fluids*. (NY): Gordon and Breach; 1976. p. 273–373.
- [5] Dozov I. On the spontaneous symmetry breaking in the mesophases of achiral banana-shaped molecules. *Europhy Lett*. 2001;56(2):247–253. doi: [10.1209/epl/i2001-00513-x](https://doi.org/10.1209/epl/i2001-00513-x)
- [6] Henderson PA, Imrie CT. Methylene-linked liquid crystal dimers and the twist-bend nematic phase. *Liq Cryst*. 2011;38(11–12):1407–1414. doi: [10.1080/02678292.2011.624368](https://doi.org/10.1080/02678292.2011.624368)
- [7] Dawood AA, Grossel MC, Luckhurst GR, et al. Twist-bend nematics, liquid crystal dimers, structure-property relations. *Liq Cryst*. 2017;44:106–126.
- [8] Dawood AA, Grossel MC, Luckhurst GR, et al. On the twist-bend nematic phase formed directly from the isotropic phase. *Liq Cryst*. 2016;43(1):2–12. doi: [10.1080/02678292.2015.1114158](https://doi.org/10.1080/02678292.2015.1114158)
- [9] Lesac A, Baumeister U, Dokli I, et al. Geometric aspects influencing N-N TB transition - implication of intramolecular torsion. *Liq Cryst*. 2018;45(7):1101–1110. doi: [10.1080/02678292.2018.1453556](https://doi.org/10.1080/02678292.2018.1453556)
- [10] Knezevic A, Dokli I, Novak J, et al. Fluorinated twist-bend nematogens: the role of intermolecular interaction. *Liq Cryst*. 2021;48(5):756–766. doi: [10.1080/02678292.2020.1817585](https://doi.org/10.1080/02678292.2020.1817585)
- [11] Panov VP, Vij JK, Mehl GH. Twist-bend nematic phase in cyanobiphenyls and difluoroterphenyls bimesogens. *Liq Cryst*. 2017;44:147–159.
- [12] Arakawa Y, Ishida Y, Komatsu K, et al. Thioether-linked benzylideneaniline-based twist-bend nematic liquid crystal dimers: insights into spacer lengths, mesogenic arm structures, and linkage types. *Tetrahedron*. 2021;95:132351. doi: [10.1016/j.tet.2021.132351](https://doi.org/10.1016/j.tet.2021.132351)
- [13] Arakawa Y, Komatsu K, Shiba T, et al. Methylene- and thioether-linked cyanobiphenyl-based liquid crystal dimers $CBnSCB$ exhibiting room temperature

- twist-bend nematic phases and glasses. *Mater Adv.* 2021;2(5):1760–1773. doi: [10.1039/D0MA00990C](https://doi.org/10.1039/D0MA00990C)
- [14] Arakawa Y, Komatsu K, Ishida Y, et al. Carbonyl- and thioether-linked cyanobiphenyl-based liquid crystal dimers exhibiting twist-bend nematic phases. *Tetrahedron.* 2021;81:131870. doi: [10.1016/j.tet.2020.131870](https://doi.org/10.1016/j.tet.2020.131870)
- [15] Arakawa Y, Komatsu K, Ishida Y, et al. Thioether-linked azobenzene-based liquid crystal dimers exhibiting the twist-bend nematic phase over a wide temperature range. *Liq Cryst.* 2021;48(5):641–652. doi: [10.1080/02678292.2020.1800848](https://doi.org/10.1080/02678292.2020.1800848)
- [16] Mandle RJ. A Ten-year perspective on twist-bend nematic materials. *Molecules.* 2022;27(9):2689. doi: [10.3390/molecules27092689](https://doi.org/10.3390/molecules27092689)
- [17] Archbold CT, Andrews JL, Mandle RJ, et al. Effect of the linking unit on the twist-bend nematic phase in liquid crystal dimers: a comparative study of two homologous series of methylene- and ether-linked dimers. *Liq Cryst.* 2017;44:84–92. doi: [10.1080/02678292.2016.1240247](https://doi.org/10.1080/02678292.2016.1240247)
- [18] Mandle RJ. Designing liquid-crystalline oligomers to exhibit twist-bend modulated nematic phases. *Chem Rec.* 2018;18(9):1341–1349. doi: [10.1002/tcr.201800010](https://doi.org/10.1002/tcr.201800010)
- [19] Paterson DA, Gao M, Kim YK, et al. Understanding the twist-bend nematic phase: the characterisation of 1-(4-cyanobiphenyl-4'-yloxy)-6-(4-cyanobiphenyl-4'-yl)hexane (CB6OCB) and comparison with CB7CB. *Soft Matter.* 2016;12(32):6827–6840. doi: [10.1039/C6SM00537C](https://doi.org/10.1039/C6SM00537C)
- [20] Paterson DA, Xiang J, Singh G, et al. Reversible isothermal twist-bend nematic-nematic phase transition driven by the photoisomerization of an azobenzene-based nonsymmetric liquid crystal dimer. *J Am Chem Soc.* 2016;138(16):5283–5289. doi: [10.1021/jacs.5b13331](https://doi.org/10.1021/jacs.5b13331)
- [21] Paterson DA, Walker R, Abberley JP, et al. Azobenzene-based liquid crystal dimers and the twist-bend nematic phase. *Liq Cryst.* 2017;44:2060–2078. doi: [10.1080/02678292.2017.1366075](https://doi.org/10.1080/02678292.2017.1366075)
- [22] Forsyth E, Paterson DA, Cruickshank E, et al. Liquid crystal dimers and the twist-bend nematic phase: on the role of spacers and terminal alkyl chains. *J Molec Liq.* 2020;320:114391. doi: [10.1016/j.molliq.2020.114391](https://doi.org/10.1016/j.molliq.2020.114391)
- [23] Walker R, Majewska M, Pocięcha D, et al. Twist-bend nematic glasses: the synthesis and characterisation of pyrene-based nonsymmetric dimers. *Chemphyschem.* 2021;22(5):461–470. doi: [10.1002/cphc.202000993](https://doi.org/10.1002/cphc.202000993)
- [24] Walker R, Pocięcha D, Strachan GJ, et al. Molecular curvature, specific intermolecular interactions and the twist-bend nematic phase: the synthesis and characterisation of the 1-(4-cyanobiphenyl-4'-yl)-6-(4-alkylanilinebenzylidene-4'-oxy)hexanes (CB6O.m). *Soft Matter.* 2019;15(15):3188–3197. doi: [10.1039/C9SM00026G](https://doi.org/10.1039/C9SM00026G)
- [25] Cruickshank E, Salamonczyk M, Pocięcha D, et al. Sulfur-linked cyanobiphenyl-based liquid crystal dimers and the twist-bend nematic phase. *Liq Cryst.* 2019;46(10):1595–1609. doi: [10.1080/02678292.2019.1641638](https://doi.org/10.1080/02678292.2019.1641638)
- [26] Cruickshank E, Walker R, Strachan GJ, et al. The influence of the imine bond direction on the phase behaviour of symmetric and non-symmetric liquid crystal dimers. *J Molec Liq.* 2023;391:123226. doi: [10.1016/j.molliq.2023.123226](https://doi.org/10.1016/j.molliq.2023.123226)
- [27] Abberley JP, Storey JMD, Imrie CT. Structure-property relationships in azobenzene-based twist-bend nematogens. *Liq Cryst.* 2019;46(13–14):2102–2114. doi: [10.1080/02678292.2019.1643935](https://doi.org/10.1080/02678292.2019.1643935)
- [28] Majewska MM, Forsyth E, Pocięcha D, et al. Controlling spontaneous chirality in achiral materials: liquid crystal oligomers and the heliconical twist-bend nematic phase. *Chem Commun.* 2022;58(34):5285–5288. doi: [10.1039/D1CC07012F](https://doi.org/10.1039/D1CC07012F)
- [29] Tuchband MR, Paterson DA, Salamonczyk M, et al. Distinct differences in the nanoscale behaviors of the twist-bend liquid crystal phase of a flexible linear trimer and homologous dimer. *Proc Natl Acad Sci USA.* 2019;116(22):10698–10704. doi: [10.1073/pnas.1821372116](https://doi.org/10.1073/pnas.1821372116)
- [30] Mandle RJ, Goodby JW. A nanoheliconical nematic liquid crystal formed by a non-linear duplexed hexamer. *Angew Chem Int Ed.* 2018;57(24):7096–7100. doi: [10.1002/anie.201802881](https://doi.org/10.1002/anie.201802881)
- [31] Simpson FP, Mandle RJ, Moore JN, et al. Investigating the Cusp between the nano- and macro-sciences in supermolecular liquid-crystalline twist-bend nematogens. *J Mater Chem C.* 2017;5(21):5102–5110. doi: [10.1039/C7TC00516D](https://doi.org/10.1039/C7TC00516D)
- [32] Al-Janabi A, Mandle RJ, Goodby JW. Isomeric trimesogens exhibiting modulated nematic mesophases. *RSC Adv.* 2017;7(75):47235–47242. doi: [10.1039/C7RA10261E](https://doi.org/10.1039/C7RA10261E)
- [33] Arakawa Y, Komatsu K, Inui S, et al. Thioether-linked liquid crystal dimers and trimers: the twist-bend nematic phase. *J Molec Str.* 2020;1199:126913. doi: [10.1016/j.molstruc.2019.126913](https://doi.org/10.1016/j.molstruc.2019.126913)
- [34] Arakawa Y, Komatsu K, Shiba T, et al. Phase behaviors of classic liquid crystal dimers and trimers: alternate induction of smectic and twist-bend nematic phases depending on spacer parity for liquid crystal trimers. *J Molec Liq.* 2021;326:115319. doi: [10.1016/j.molliq.2021.115319](https://doi.org/10.1016/j.molliq.2021.115319)
- [35] Arakawa Y, Komatsu K, Ishida Y, et al. Thioether-linked liquid crystal trimers: odd-even effects of spacers and the influence of thioether bonds on phase behavior. *Materials.* 2022;15(5):1709. doi: [10.3390/ma15051709](https://doi.org/10.3390/ma15051709)
- [36] Chen D, Nakata M, Shao RF, et al. Twist-bend heliconical chiral nematic liquid crystal phase of an achiral rigid bent-core mesogen. *Phys Rev E.* 2014;89(2):022506. doi: [10.1103/PhysRevE.89.022506](https://doi.org/10.1103/PhysRevE.89.022506)
- [37] Sreenilayam SP, Panov VP, Vij JK, et al. The N-TB phase in an achiral asymmetrical bent-core liquid crystal terminated with symmetric alkyl chains. *Liq Cryst.* 2017;44:244–253. doi: [10.1080/02678292.2016.1253878](https://doi.org/10.1080/02678292.2016.1253878)
- [38] Walker R, Pocięcha D, Crawford CA, et al. Hydrogen bonding and the design of twist-bend nematogens. *J Molec Liq.* 2020;303:112630. doi: [10.1016/j.molliq.2020.112630](https://doi.org/10.1016/j.molliq.2020.112630)
- [39] Walker R, Pocięcha D, Martinez-Felipe A, et al. Twist-Bend nematogenic supramolecular dimers and trimers formed by hydrogen bonding. *Crystals.* 2020;10(3):175. doi: [10.3390/cryst10030175](https://doi.org/10.3390/cryst10030175)

- [40] Walker R, Pocięcha D, Abberley JP, et al. Spontaneous chirality through mixing achiral components: a twist-bend nematic phase driven by hydrogen-bonding between unlike components. *Chem Commun.* 2018;54(27):3383–3386. doi: [10.1039/C8CC00525G](https://doi.org/10.1039/C8CC00525G)
- [41] Walker R. The twist-bend phases: structure–property relationships, chirality and hydrogen-bonding. *Liq Cryst Today.* 2020;29(1):2–14. doi: [10.1080/1358314X.2020.1771841](https://doi.org/10.1080/1358314X.2020.1771841)
- [42] Jansze SM, Martinez-Felipe A, Storey JMD, et al. A twist-bend nematic phase driven by hydrogen bonding. *Angew Chem Int Ed.* 2015;54(2):643–646. doi: [10.1002/anie.201409738](https://doi.org/10.1002/anie.201409738)
- [43] Stevenson WD, An JG, Zeng XB, et al. Twist-bend nematic phase in biphenylethane-based copolyethers. *Soft Matter.* 2018;14(16):3003–3011. doi: [10.1039/C7SM02525D](https://doi.org/10.1039/C7SM02525D)
- [44] Tufaha N, Gibb CJ, Storey JMD, et al. Can even-membered liquid crystal dimers exhibit the twist-bend nematic phase? The preparation and properties of disulphide and thioether linked dimers. *Liq Cryst.* 2023;50(7–10):1362–1374. doi: [10.1080/02678292.2023.2242824](https://doi.org/10.1080/02678292.2023.2242824)
- [45] Archbold CT, Davis EJ, Mandle RJ, et al. Chiral dopants and the twist-bend nematic phase – induction of novel mesomorphic behaviour in an apolar bimesogen. *Soft Matter.* 2015;11(38):7547–7557. doi: [10.1039/C5SM01935D](https://doi.org/10.1039/C5SM01935D)
- [46] Walker R, Pocięcha D, Salamonczyk M, et al. Intrinsically chiral Twist-Bend Nematogens: interplay of molecular and structural chirality in the N TB phase. *Chemphyschem.* 2023;24(6):e202300105. doi: [10.1002/cphc.202300105](https://doi.org/10.1002/cphc.202300105)
- [47] Walker R, Pocięcha D, Salamonczyk M, et al. Supramolecular liquid crystals exhibiting a chiral twist-bend nematic phase. *Materials advances.* 2020;1(6):1622–1630. doi: [10.1039/D0MA00302F](https://doi.org/10.1039/D0MA00302F)
- [48] Walker R, Pocięcha D, Storey JMD, et al. The chiral twist-bend nematic phase (N*TB). *Chem Eur J.* 2019;25(58):13329–13335. doi: [10.1002/chem.201903014](https://doi.org/10.1002/chem.201903014)
- [49] Imrie CT, Walker R, Storey JMD, et al. Liquid crystal dimers and smectic phases from the intercalated to the twist-bend. *Crystals.* 2022;12(9):1245. doi: [10.3390/cryst12091245](https://doi.org/10.3390/cryst12091245)
- [50] Alshammari AF, Pocięcha D, Walker R, et al. New patterns of twist-bend liquid crystal phase behaviour: the synthesis and characterisation of the 1-(4-cyanobiphenyl-4'-yl)-10-(4-alkylaniline-benzylidene-4'-oxy) decanes (CB10O-m). *Soft Matter.* 2022;18(25):4679–4688. doi: [10.1039/D2SM00162D](https://doi.org/10.1039/D2SM00162D)
- [51] Pocięcha D, Vaupotic N, Majewska M, et al. Photonic bandgap in achiral liquid crystals—A twist on a twist. *Adv Mater.* 2021;33(39):2103288. doi: [10.1002/adma.202103288](https://doi.org/10.1002/adma.202103288)
- [52] Salamonczyk M, Vaupotic N, Pocięcha D, et al. Multi-level chirality in liquid crystals formed by achiral molecules. *Nat Commun.* 2019;10(1):1922. doi: [10.1038/s41467-019-09862-y](https://doi.org/10.1038/s41467-019-09862-y)
- [53] Abberley JP, Killah R, Walker R, et al. Helical smectic phases formed by achiral molecules. *Nat Commun.* 2018;9(1):228. doi: [10.1038/s41467-017-02626-6](https://doi.org/10.1038/s41467-017-02626-6)
- [54] Cruickshank E, Anderson K, Storey JMD, et al. Helical phases assembled from achiral molecules: twist-bend nematic and helical filamentary B-4 phases formed by mesogenic dimers. *J Molec Liq.* 2022;346:118180. doi: [10.1016/j.molliq.2021.118180](https://doi.org/10.1016/j.molliq.2021.118180)
- [55] Meyer C, Davidson P, Luckhurst GR, et al. Temperature dependence of the electroclinic effect in the twist-bend nematic phase. *Crystals.* 2023;13(3):465. doi: [10.3390/cryst13030465](https://doi.org/10.3390/cryst13030465)
- [56] Sellares J, Diego JA, Lopez DO, et al. Comparative dielectric and thermally stimulated-depolarization-current studies of the liquid crystal dimers 1'',9''-bis(4-cyanobiphenyl-4'-yl) nonane and heptane and a binary mixture between them, close to the glass transition. *Phys Rev E.* 2022;106(5):054702. doi: [10.1103/PhysRevE.106.054702](https://doi.org/10.1103/PhysRevE.106.054702)
- [57] Oswald P, Poy G, Krishnamurthy KS. Structure and Lehmann rotation of drops in a surfactant-doped bent-core liquid crystal. *Phys Rev E.* 2022;106(2):024705. doi: [10.1103/PhysRevE.106.024705](https://doi.org/10.1103/PhysRevE.106.024705)
- [58] Yu G, Wilson MR. All-atom simulations of bent liquid crystal dimers: the twist-bend nematic phase and insights into conformational chirality. *Soft Matter.* 2022;18(15):3087–3096. doi: [10.1039/D2SM00291D](https://doi.org/10.1039/D2SM00291D)
- [59] Dunmur D. Anatomy of a discovery: the twist-bend nematic phase. *Crystals.* 2022;12(3):309. doi: [10.3390/cryst12030309](https://doi.org/10.3390/cryst12030309)
- [60] Ferrarini A, Greco C, Luckhurst GR, et al. Exploring the behaviour of the twist-bend nematic phase using NMR with a variety of spin probes. *Liq Cryst.* 2020;47(13):2074–2091. doi: [10.1080/02678292.2020.1769756](https://doi.org/10.1080/02678292.2020.1769756)
- [61] Krishnamurthy KS, Rao DSS, Khatavi SY, et al. Twist-bend nematic drops as colloidal particles: electric instabilities. *Phys Rev E.* 2023;107(4):044703. doi: [10.1103/PhysRevE.107.044703](https://doi.org/10.1103/PhysRevE.107.044703)
- [62] Imrie CT, Paterson DA, Storey JMD, et al. Phase transitions in a high magnetic field of an odd, symmetric liquid crystal dimer having two nematic phases, N U and N TB, studied by NMR spectroscopy. *Phys Rev E.* 2020;102(4):042706. doi: [10.1103/PhysRevE.102.042706](https://doi.org/10.1103/PhysRevE.102.042706)
- [63] Luckhurst GR, Timimi BA, Wells NJ, et al. On orientational order in nematic and twist-bend nematic phases: a 2 H-NMR study of binary mixtures of the odd dimer, 1'',9''-bis(4-cyanobiphenyl-4'-yl) nonane, (CB9CB), and the monomer, 4-pentyl-4'-cyanobiphenyl, (5CB-d2). *Liq Cryst.* 2018;45(13–15):1913–1928. doi: [10.1080/02678292.2018.1533597](https://doi.org/10.1080/02678292.2018.1533597)
- [64] Iadlovská OS, Babakhanova G, Mehl GH, et al. Temperature dependence of bend elastic constant in oblique helicoidal cholesterics. *Phys Rev Res.* 2020;2(1):013248. doi: [10.1103/PhysRevResearch.2.013248](https://doi.org/10.1103/PhysRevResearch.2.013248)
- [65] Joshi V, Paterson DA, Storey JMD, et al. Tunable back-flow in chiral nematic liquid crystals via twist-bend nematogens and surface-localised in-situ polymer protrusions. *Liq Cryst.* 2017;44(14–15):2327–2336. doi: [10.1080/02678292.2017.1374479](https://doi.org/10.1080/02678292.2017.1374479)
- [66] Mandle RJ, Davis EJ, Archbold CT, et al. Microscopy studies of the nematic N TB phase of 1,11-di-(1'

- '-cyanobiphenyl-4-yl)undecane. *J Mater Chem C*. 2014;2(3):556–566. doi: [10.1039/C3TC32137A](https://doi.org/10.1039/C3TC32137A)
- [67] Paterson DA, Abberley JP, Harrison WT, et al. Cyanobiphenyl-based liquid crystal dimers and the twist-bend nematic phase. *Liq Cryst*. 2017;44:127–146. doi: [10.1080/02678292.2016.1274293](https://doi.org/10.1080/02678292.2016.1274293)
- [68] Paterson DA, Walker R, Storey JMD, et al. Molecular structure and the twist-bend nematic phase: the role of spacer length in liquid crystal dimers. *Liq Cryst*. 2023;50(4):725–736. doi: [10.1080/02678292.2023.2198505](https://doi.org/10.1080/02678292.2023.2198505)
- [69] Ramou E, Welch C, Hussey J, et al. The induction of the N_{tb} phase in mixtures. *Liq Cryst*. 2018;45(13–15):1929–1935. doi: [10.1080/02678292.2018.1524523](https://doi.org/10.1080/02678292.2018.1524523)
- [70] Arakawa Y, Arai Y, Horita K, et al. Twist-bend nematic phase behavior of cyanobiphenyl-based dimers with propane, ethoxy, and ethylthio spacers. *Crystals*. 2022;12(12):1734. doi: [10.3390/cryst12121734](https://doi.org/10.3390/cryst12121734)
- [71] Luckhurst GR. Liquid crystals: a chemical physicist's view. *Liq Cryst*. 2005;32:1335–1364. doi: [10.1080/02678290500423128](https://doi.org/10.1080/02678290500423128)
- [72] Emsley JW, Luckhurst GR, Shilstone GN, et al. The preparation and properties of the α,ω -bis(4,4'-cyanobiphenyloxy)Alkanes: nematogenic molecules with a flexible core. *Molec Cryst Liq Cryst*. 1984;102(8–9):223–233. doi: [10.1080/01406568408070532](https://doi.org/10.1080/01406568408070532)
- [73] Babakhanova G, Parsouzi Z, Paladugu S, et al. Elastic and viscous properties of the nematic dimer CB7CB. *Phys Rev E*. 2017;96(6):062704. doi: [10.1103/PhysRevE.96.062704](https://doi.org/10.1103/PhysRevE.96.062704)
- [74] Cestari M, Frezza E, Ferrarini A, et al. Crucial role of molecular curvature for the bend elastic and flexoelectric properties of liquid crystals: mesogenic dimers as a case study. *Journal of Materials Chemistry*. 2011;21(33):12303–12308. doi: [10.1039/c1jm12233a](https://doi.org/10.1039/c1jm12233a)
- [75] Xiang J, Shiyankovskii SV, Imrie CT, et al. Electrooptic response of chiral nematic liquid crystals with oblique helicoidal director. *Phys Rev Lett*. 2014;112(21):217801. doi: [10.1103/PhysRevLett.112.217801](https://doi.org/10.1103/PhysRevLett.112.217801)
- [76] Xiang J, Li YN, Li Q, et al. Electrically tunable selective reflection of light from ultraviolet to visible and infrared by Helicoidal Cholesterics. *Adv Mater*. 2015;27(19):3014–3018. doi: [10.1002/adma.201500340](https://doi.org/10.1002/adma.201500340)
- [77] Iadlovská OS, Thapa K, Rajabi M, et al. In situ measurements of twist and bend elastic constants in the oblique helicoidal cholesteric. *Phys Rev E*. 2022;106(2):024702. doi: [10.1103/PhysRevE.106.024702](https://doi.org/10.1103/PhysRevE.106.024702)
- [78] DeGennes PG. Calculation of distortion in a cholesteric structure by a magnetic field. *Solid State Commun*. 1968;6(3):163–165. doi: [10.1016/0038-1098\(68\)90024-0](https://doi.org/10.1016/0038-1098(68)90024-0)
- [79] Meyer RB. Effects of electric and magnetic fields on structure of cholesteric liquid crystals. *Appl Phys Lett*. 1968;12(9):281–282. doi: [10.1063/1.1651992](https://doi.org/10.1063/1.1651992)
- [80] Miyaura N, Yanagi T, Suzuki A. The palladium-catalyzed cross-coupling reaction of phenylboronic acid with haloarenes in the presence of bases. *Synth Commun*. 1981;11(7):513–519. doi: [10.1080/00397918108063618](https://doi.org/10.1080/00397918108063618)
- [81] Kanagarajan V, Thanusu J, Gopalakrishnan M. Synthesis and in vitro microbiological evaluation of an array of biolabile 2-morpholino-N-(4,6-diarylpyrimidin-2-yl)acetamides. *Eur J Med Chem*. 2010;45(4):1583–1589. doi: [10.1016/j.ejmech.2009.12.068](https://doi.org/10.1016/j.ejmech.2009.12.068)
- [82] Obaza J, Smith FX. A malonic ester synthesis with acid-chlorides - the homologation of dioic acids. *Synth Commun*. 1982;12(1):19–23. doi: [10.1080/00397918208080061](https://doi.org/10.1080/00397918208080061)
- [83] Frisch MJ, Trucks GW, Schlegel HB, et al. Gaussian 09. Wallingford (CT): Gaussian Inc.; 2016 (Revision D.01).
- [84] Dennington R, Keith T, Gauss View MJ. Version 5. Shawnee Mission (KS): Semichem Inc; 2009.
- [85] Tarini M, Cignoni P, Montani C. Ambient occlusion and edge cueing to enhance real time molecular visualization. *IEEE Trans Vis Comp Graphics*. 2006;12(5):1237–1244. doi: [10.1109/TVCG.2006.115](https://doi.org/10.1109/TVCG.2006.115)
- [86] Kedzierski J, Raszewski Z, Kojdecki MA, et al. Determination of ordinary and extraordinary refractive indices of nematic liquid crystals by using wedge cells. *Opto-Electron Rev*. 2010;18(2):214–218. doi: [10.2478/s11772-010-0009-8](https://doi.org/10.2478/s11772-010-0009-8)
- [87] Nastishin YA, Polak RD, Shiyankovskii SV, et al. Nematic polar anchoring strength measured by electric field techniques. *J Appl Phys*. 1999;86(8):4199–4213. doi: [10.1063/1.371347](https://doi.org/10.1063/1.371347)
- [88] Salamonczyk M, Vaupotic N, Pocięcha D, et al. Structure of nanoscale-pitch helical phases: blue phase and twist-bend nematic phase resolved by resonant soft X-ray scattering. *Soft Matter*. 2017;13(38):6694–6699. doi: [10.1039/C7SM00967D](https://doi.org/10.1039/C7SM00967D)
- [89] Saha R, Feng C, Welch C, et al. The interplay between spatial and helical orientational order in twist-bend nematic materials. *Phys Chem Chem Phys*. 2021;23(7):4055–4063. doi: [10.1039/D0CP06633H](https://doi.org/10.1039/D0CP06633H)
- [90] Arakawa Y, Komatsu K, Feng J, et al. Distinct twist-bend nematic phase behaviors associated with the ester-linkage direction of thioether-linked liquid crystal dimers. *Mater Adv*. 2021;2(1):261–272. doi: [10.1039/D0MA00746C](https://doi.org/10.1039/D0MA00746C)
- [91] Humphries RL, Luckhurst GR. Statistical-theory of liquid-crystalline mixtures - components of different size. *Chem Phys Lett*. 1973;23(4):567–570. doi: [10.1016/0009-2614\(73\)89030-X](https://doi.org/10.1016/0009-2614(73)89030-X)
- [92] Arakawa Y, Horita K, Igawa K. Phase behaviour of ester-linked cyanobiphenyl dimers and fluorinated analogues: the direct isotropic to twist-bend nematic phase transition. *Liq Cryst*. 2023;50(13–14):2216–2228. doi: [10.1080/02678292.2023.2241039](https://doi.org/10.1080/02678292.2023.2241039)
- [93] Wang DL, Liu J, Zhao WG, et al. Facile synthesis of liquid crystal dimers bridged with a phosphonic group. *Chem Eur J*. 2022;28(70):e2022021. doi: [10.1002/chem.202202146](https://doi.org/10.1002/chem.202202146)
- [94] Challa PK, Borshch V, Parri O, et al. Twist-bend nematic liquid crystals in high magnetic fields. *Phys Rev E*. 2014;89(6):060501. doi: [10.1103/PhysRevE.89.060501](https://doi.org/10.1103/PhysRevE.89.060501)
- [95] Parsouzi Z, Pardaev SA, Welch C, et al. Light scattering study of the “pseudo-layer” compression elastic constant in a twist-bend nematic liquid crystal. *Phys Chem Chem Phys*. 2016;18(46):31645–31652. doi: [10.1039/C6CP06292J](https://doi.org/10.1039/C6CP06292J)
- [96] Sarker P, Mandal P, Paul S, et al. X-ray diffraction, optical birefringence, dielectric and phase transition properties of the long homologous series of nematogens 4-(*trans*-4'-*n*-alkylcyclohexyl) isothiocyantobenzenes.

- Liq Cryst. 2003;30(4):507–527. doi: [10.1080/0267829031000091156](https://doi.org/10.1080/0267829031000091156)
- [97] Imrie CT, Henderson PA. Liquid crystal dimers and higher oligomers: between monomers and polymers. *Chem Soc Rev.* 2007;36(12):2096–2124. doi: [10.1039/b714102e](https://doi.org/10.1039/b714102e)
- [98] Babakhanova G, Wang H, Rajabi M, et al. Elastic and electro-optical properties of flexible fluorinated dimers with negative dielectric anisotropy. *Liq Cryst.* 2022;49(7–9):982–994. doi: [10.1080/02678292.2021.1973602](https://doi.org/10.1080/02678292.2021.1973602)
- [99] Meyer C, Luckhurst GR, Dozov I. The temperature dependence of the heliconical tilt angle in the twist-bend nematic phase of the odd dimer CB7CB. *J Mater Chem C.* 2015;3(2):318–328. doi: [10.1039/C4TC01927J](https://doi.org/10.1039/C4TC01927J)
- [100] Cukrov G, Golestani YM, Xiang J, et al. Comparative analysis of anisotropic material properties of uniaxial nematics formed by flexible dimers and rod-like monomers. *Liq Cryst.* 2017;44:219–231. doi: [10.1080/02678292.2016.1240248](https://doi.org/10.1080/02678292.2016.1240248)
- [101] Pocięcha D, Crawford CA, Paterson DA, et al. Critical behavior of the optical birefringence at the nematic to twist-bend nematic phase transition. *Phys Rev E.* 2018;98(5):052706. doi: [10.1103/PhysRevE.98.052706](https://doi.org/10.1103/PhysRevE.98.052706)
- [102] Adlem K, Copic M, Luckhurst GR, et al. Chemically induced twist-bend nematic liquid crystals, liquid crystal dimers, and negative elastic constants. *Phys Rev E.* 2013;88(2):022503. doi: [10.1103/PhysRevE.88.022503](https://doi.org/10.1103/PhysRevE.88.022503)
- [103] Greco C, Luckhurst GR, Ferrarini A. Molecular geometry, twist-bend nematic phase and unconventional elasticity: a generalised Maier–saupe theory. *Soft Matter.* 2014;10(46):9318–9323. doi: [10.1039/C4SM02173H](https://doi.org/10.1039/C4SM02173H)
- [104] Henderson PA, Niemeyer O, Imrie CT. Methylene-linked liquid crystal dimers. *Liq Cryst.* 2001;28(3):463–472. doi: [10.1080/02678290010007558](https://doi.org/10.1080/02678290010007558)
- [105] Henderson PA, Seddon JM, Imrie CT. Methylene- and ether-linked liquid crystal dimers II. Effects of mesogenic linking unit and terminal chain length. *Liq Cryst.* 2005;32(11–12):1499–1513. doi: [10.1080/02678290500284983](https://doi.org/10.1080/02678290500284983)
- [106] Emerson APJ, Luckhurst GR. On the relative propensities of ether and methylene linkages for liquid-crystal formation in calamitics. *Liq Cryst.* 1991;10(6):861–868. doi: [10.1080/02678299108036460](https://doi.org/10.1080/02678299108036460)
- [107] Ferrarini A, Luckhurst GR, Nordio PL, et al. Understanding the dependence of the transitional properties of liquid crystal dimers on their molecular geometry. *Liq Cryst.* 1996;21(3):373–382. doi: [10.1080/02678299608032846](https://doi.org/10.1080/02678299608032846)
- [108] Ferrarini A, Luckhurst GR, Nordio PL, et al. Prediction of the transitional properties of liquid-crystal dimers - a molecular-field calculation based on the surface tensor parametrization. *J Chem Phys.* 1994;100(2):1460–1469. doi: [10.1063/1.466625](https://doi.org/10.1063/1.466625)

Cyanobiphenyl-based liquid crystal dimers and the twist-bend nematic phase: on the role played by the length and parity of the spacer

Ewan Cruickshank^a, Grant J Strachan^a, Kamal Thapa^{b,c}, Damian Pocięcha^d, Mirosław Salamończyk^d, John MD Storey^a, Ewa Gorecka^d, Oleg D. Lavrentovich^{b,c,e} and Corrie T Imrie^{a*}

^aDepartment of Chemistry, School of Natural and Computing Sciences, University of Aberdeen, AB24 3UE, Scotland, United Kingdom; ^bAdvanced Materials and Liquid Crystal Institute, Kent State University, Kent, Ohio 44242, USA; ^cDepartment of Physics, Kent State University, Kent, Ohio 44242, USA; ^dFaculty of Chemistry, University of Warsaw, ul. Żwirki i Wigury 101, 02-089, Warsaw, Poland; ^eMaterials Science Graduate Program, Kent State University, Kent, Ohio 44242, USA

*Author for correspondence: email: c.t.imrie@abdn.ac.uk

General Information

Reagents

All reagents and solvents that were available commercially were purchased from Sigma Aldrich, Fisher Scientific or Fluorochem and were used without further purification unless otherwise stated. Where required, solvents were dried over molecular sieves for a minimum of 24 hours prior to use.

Thin Layer Chromatography

Reactions were monitored using thin layer chromatography, and the appropriate solvent system, using aluminium-backed plates with a coating of Merck Kieselgel 60 F254 silica which were purchased from Merck KGaA. The spots on the plate were visualised by UV light (254 nm) or by oxidation using either a potassium permanganate stain or iodine dip.

Column Chromatography

For normal phase column chromatography, the separations were carried out using silica gel grade 60 Å, 40-63 µm particle size, purchased from Fluorochem and using an appropriate solvent system.

Structure Characterisation

All final products and intermediates that were synthesised were characterised using ¹H NMR, ¹³C NMR and infrared spectroscopies. The ¹H and ¹³C NMR spectra were recorded on either a 400 MHz Bruker Avance III HD NMR spectrometer, or a 300 MHz Bruker Ultrashield NMR spectrometer. The infrared spectra were recorded on a Thermal Scientific Nicolet IR100 FTIR spectrometer with an ATR diamond cell or a Perkin Elmer Spectrum 2 FTIR with an ATR diamond cell.

Purity Analysis

In order to determine the purity of the final products, elemental analysis was used. C, H, N microanalysis were carried out by the Sheffield Analytical and Scientific Services Elemental Microanalysis Service at the University of Sheffield using an Elementar Vario MICRO Cube. The instrument was calibrated using series of different masses of sulphanilamide and

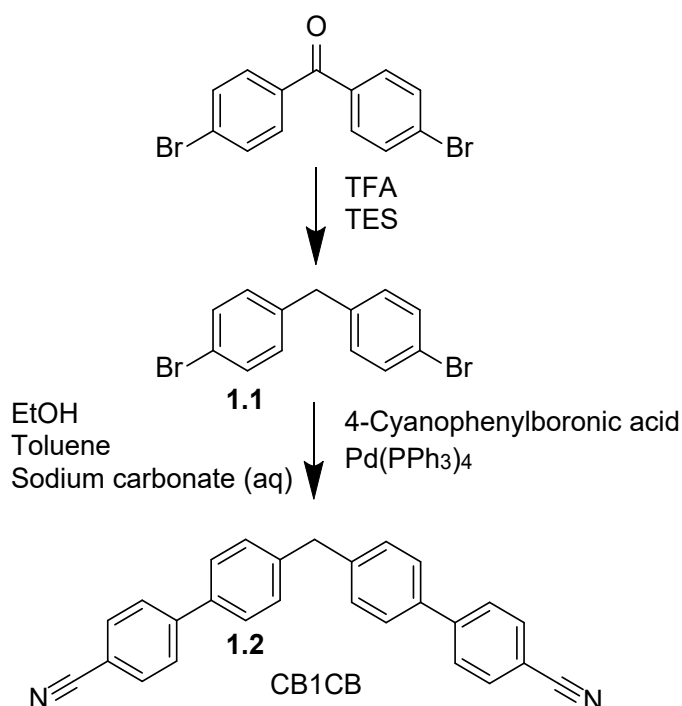
acetanilide. High-resolution mass spectrometry was carried out at the University of Aberdeen by Dr Morag Douglas using a Waters XEVO G2 Q-Tof mass spectrometer. The instrument was calibrated with sodium formate, and the lock mass was leucine enkephalin, Formula: $C_{28}H_{37}N_5O_7$, $[M+H]^+$: 556.2771.

Phase Diagrams

To construct phase diagrams in order to confirm phase assignments or to determine virtual transition temperatures, binary mixtures were prepared by co-dissolving pre-weighed masses in chloroform or dichloromethane and allowing the solvent to evaporate slowly at room temperature. Each mixture was further dried in a vacuum oven at 50 °C overnight.

Synthesis and Analytical Data

CB1CB



Scheme S11. Synthesis of CB1CB.

The synthesis of CB1CB follows the steps outlined in **Scheme S11**. CB1CB (**1.2**) was synthesised using a hydrosilane reduction¹ followed by a Suzuki-Miyaura cross-coupling reaction² to form the desired product.

1.1 1,1-Bis(4-bromophenylmethane)

To a pre-dried flask flushed with argon, 4,4'-dibromobenzophenone (1.53 g, 4.51 × 10⁻³ mol) was added and the flask was placed into an ice bath in order to maintain the temperature at 0 °C. The solid was solubilised using trifluoroacetic acid (15 mL) and dry dichloromethane (15 mL), along with stirring. Finally, triethylsilane (3 mL) was added into the flask and the ice bath was removed. The extent of the reaction was monitored by TLC using dichloromethane as the solvent system (RF value quoted in the product data) and was left overnight. The reaction mixture was added to a mixture of dichloromethane (100 mL) and water (100 mL). The organic layer was washed with water (3 × 50 mL) and dried over anhydrous magnesium sulfate. The magnesium sulfate was removed by vacuum filtration and the filtrate removed under vacuum to leave a yellow oil, which was placed in the freezer at -20 °C overnight until a white solid

formed. The solid was washed with water (3×100 mL), collected with vacuum filtration, and used without further purification.

Yield: 0.780 g, 53.0 %. RF: 0.67. MP: 58 °C

ν_{max}/cm^{-1} : 1485, 1438, 1401, 1201, 1111, 1067, 1010, 858, 807, 776, 723, 620, 492, 480

$\delta_{\text{H}}/\text{ppm}$ (400 MHz, CDCl_3): 7.43 (4 H, d, J 8.0 Hz, Ar-H), 7.05 (4 H, d, J 8.0 Hz, Ar-H), 3.90 (2 H, s, Ar- CH_2 -Ar)

$\delta_{\text{C}}/\text{ppm}$ (100 MHz, CDCl_3): 139.42, 131.65, 130.59, 120.21, 40.68

EA: Calculated for $\text{C}_{13}\text{H}_{10}\text{Br}_2$: C = 47.89 %, H = 3.09 %, Br = 49.02 %; Found: C = 47.82 %, H = 3.24 %, Br = 48.56 %

1.2 1,1-Bis-(4'-cyano-[1,1'-biphenyl]-4-yl)methane (CB1CB)

To a pre-dried flask fitted with a condenser and flushed with argon, compound **1.1** (0.730 g, 2.24×10^{-3} mol), 4-cyanophenylboronic acid (0.658 g, 4.48×10^{-3} mol) and tetrakis(triphenylphosphine)palladium(0) (0.026 g, 2.25×10^{-5} mol) were added. A mixture of aqueous sodium carbonate (2 M, 10 mL), ethanol (5 mL) and toluene (40 mL) was added and the reaction mixture was heated to 85 °C for 24 h with stirring. The reaction mixture was cooled to room temperature and 32 % hydrochloric acid (2 mL) was added dropwise until effervescence was no longer observed. The resulting mixture was filtered using vacuum filtration to remove the palladium catalyst, and the solvents were removed under vacuum. Water (100 mL) and dichloromethane (100 mL) were added to the solid obtained. The organic layer was washed with water (2×50 mL) and dried over anhydrous magnesium sulfate. The magnesium sulfate was removed by vacuum filtration and the solvents evaporated under vacuum to give a brown/tan solid. The crude product was purified using a silica gel column with 10 % 40:60 petroleum ether and 90 % dichloromethane as eluent (RF value quoted in product data). The eluent fractions of interest were evaporated under vacuum to leave a white solid which was recrystallised from hot ethanol (40 mL).

Yield: 0.351 g, 42.3 %. RF: 0.44. MP: 206 °C

ν_{max}/cm^{-1} : 2227, 1603, 1493, 1398, 1180, 1114, 1005, 838, 805, 776, 649, 548

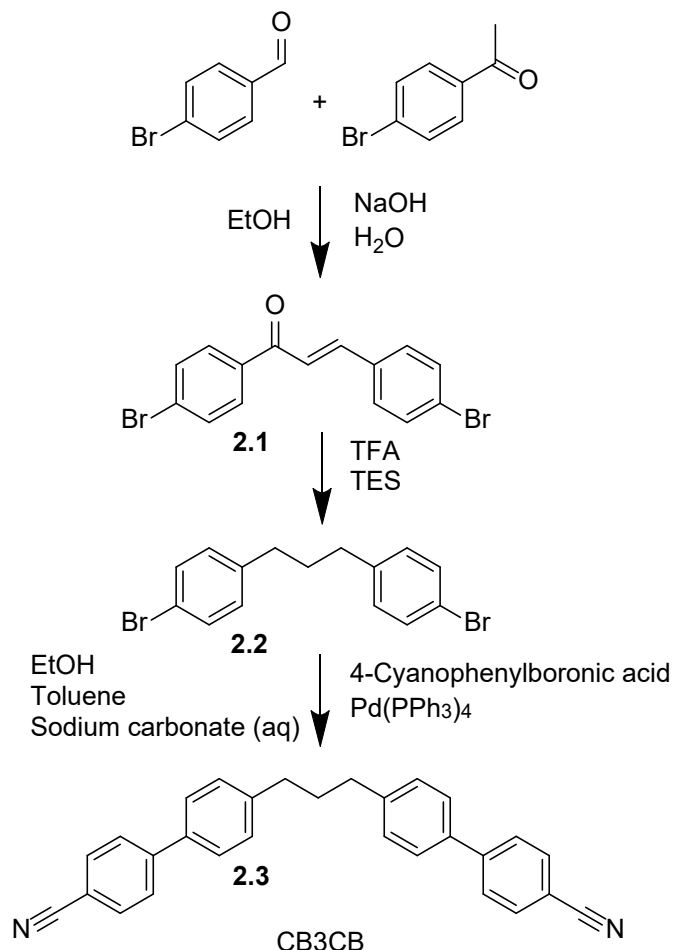
$\delta_{\text{H}}/\text{ppm}$ (400 MHz, CDCl_3): 7.74 (4 H, d, J 8.1 Hz, Ar-H), 7.69 (4 H, d, J 8.1 Hz, Ar-H), 7.57 (4 H, d, J 8.0 Hz, Ar-H), 7.36 (4 H, d, J 8.0 Hz, Ar-H), 4.12 (2 H, s, Ar- CH_2 -Ar)

$\delta_{\text{C}}/\text{ppm}$ (100 MHz, CDCl_3): 145.32, 141.40, 137.22, 132.62, 129.69, 127.54, 127.45, 118.95, 110.80, 41.27

EA: Calculated for $\text{C}_{27}\text{H}_{18}\text{N}_2$: C = 87.54 %, H = 4.90 %, N = 7.56 %; Found: C = 87.05 %, H = 4.98 %, N = 7.38 %

MS (ESI+, m/z) = $[M+Na]^+$: Calculated for $C_{27}H_{18}N_2Na$: 393.1369; Found: 393.1368.
Difference: 0.3 ppm.

CB3CB



Scheme 3.2. Synthesis of CB3CB.

The synthesis of CB3CB follows the steps outlined in **Scheme SI2**. CB3CB (**2.3**) was synthesised using an aldol condensation,³ followed by a hydrosilane reduction¹ and then by a Suzuki-Miyaura cross-coupling reaction² to form the desired product.

2.1 2E-1,3-Bis(4-bromophenyl)prop-2-en-1-one

To a pre-dried flask flushed with argon, 4-bromobenzaldehyde (4.03 g, 0.0216 mol) was added along with 4-bromoacetophenone (4.41 g, 0.0221 mol) and solubilised by ethanol (100 mL). Sodium hydroxide (1.26 g, 0.315 mol) in water (30 mL), sonicated to ensure all the solid was dissolved, was added to the flask, and stirred at room temperature for 1 h. The extent of the reaction was monitored by TLC using dichloromethane as the solvent system (RF value quoted

in the product data). A yellow solid precipitated and at the end of the reaction this was collected using vacuum filtration. The solid was dried at 50 °C in a vacuum oven and used without further purification.

Yield: 7.51 g, 94.9 %. RF: 0.77. MP: 183 °C

ν_{max}/cm^{-1} : 1655, 1601, 1581, 1560, 1487, 1401, 1322, 1216, 1069, 1033, 1007, 983, 832, 811, 794, 739, 492

$\delta_{\text{H}}/\text{ppm}$ (400 MHz, CDCl_3): 7.90 (2 H, d, J 8.5 Hz, Ar-H), 7.76 (1 H, d, J 15.6 Hz, C(=O)-CH=CH-Ar), 7.67 (2 H, d, J 8.5 Hz, Ar-H), 7.58 (2 H, d, J 8.6 Hz, Ar-H), 7.52 (2 H, d, J 8.6 Hz, Ar-H), 7.48 (1 H, d, J 15.6 Hz, C(=O)-CH=CH-Ar)

$\delta_{\text{C}}/\text{ppm}$ (100 MHz, CDCl_3): 189.09, 143.96, 136.71, 133.59, 132.28, 132.00, 130.02, 129.85, 128.12, 125.08, 121.93

Data consistent with reported values ⁴

2.2 1,3-Bis(4-bromophenylpropane)

To a pre-dried flask flushed with argon placed into an ice bath in order to maintain the temperature at 0 °C, compound **2.1** (5.97 g, 0.0163 mol) was added. The solid was solubilised using trifluoroacetic acid (60 mL) and dry dichloromethane (60 mL), along with stirring. Finally, triethylsilane (26 mL) was syringed into the flask and the ice bath was removed. The extent of the reaction was monitored by TLC using dichloromethane as the solvent system (RF value quoted in the product data) and was left overnight. The reaction mixture was added to a mixture of dichloromethane (200 mL) and water (300 mL). The organic layer was washed with water (3 × 50 mL) and dried over anhydrous magnesium sulfate. The magnesium sulfate was removed by vacuum filtration and the filtrate collected. The solvent was evaporated under vacuum to leave a yellow oil, which was placed in the freezer at -20 °C overnight until a white solid formed. The solid was washed with water (3 × 100 mL), collected with vacuum filtration, and used without further purification.

Yield: 3.12 g, 54.0 %. RF: 0.85. MP: 58 °C

ν_{max}/cm^{-1} : 2940, 2857, 1486, 1459, 1402, 1149, 1069, 1009, 802, 715, 608, 497

$\delta_{\text{H}}/\text{ppm}$ (400 MHz, CDCl_3): 7.42 (4 H, d, J 8.0 Hz, Ar-H), 7.06 (4 H, d, J 8.0 Hz, Ar-H), 2.61 (4 H, t, J 7.7 Hz, Ar-CH₂-CH₂-), 1.93 (2 H, quin, J 7.7 Hz, Ar-CH₂-CH₂-CH₂-)

$\delta_{\text{C}}/\text{ppm}$ (100 MHz, CDCl_3): 140.90, 131.40, 130.17, 119.56, 34.64, 32.58

Data consistent with reported values ⁵

2.3 1,3-Bis(4'-cyano-[1,1'-biphenyl]-4-yl)propane (CB3CB)

To a pre-dried flask fitted with a condenser and flushed with argon, compound **2.2** (1.81 g, 5.08×10^{-3} mol), 4-cyanophenylboronic acid (1.73 g, 0.0117 mol) and tetrakis(triphenylphosphine)palladium(0) (0.059 g, 5.11×10^{-5} mol) were added. A mixture of aqueous sodium carbonate (2 M, 20 mL), ethanol (10 mL) and toluene (80 mL) was added, and the reaction mixture was heated to 85 °C for 24 h with stirring. The reaction mixture was cooled to room temperature and 32 % hydrochloric acid (2 mL) was added dropwise until effervescence was no longer observed. The resulting mixture was filtered using vacuum filtration to remove the palladium catalyst, and the solvents were removed under vacuum. Water (100 mL) and dichloromethane (100 mL) were added to the solid obtained. The organic layer was washed with water (2 × 50 mL) and dried over anhydrous magnesium sulfate. The magnesium sulfate was removed by vacuum filtration and the solvents evaporated under vacuum to leave a brown solid. The crude product was purified using a silica gel column with 10 % 40:60 petroleum ether and 90 % dichloromethane as eluent (RF value quoted in product data). The eluent fractions of interest were evaporated under vacuum to leave a white solid which was recrystallised from hot ethanol (50 mL).

Yield: 0.287 g, 14.2 %. RF: 0.36

T_{CrI} 141 °C $T_{\text{N}^{\text{TB}}\text{I}}$ (47 °C)

$\nu_{\text{max}}/\text{cm}^{-1}$: 2227, 1603, 1493, 1398, 1180, 1114, 1005, 838, 805, 776, 649, 548

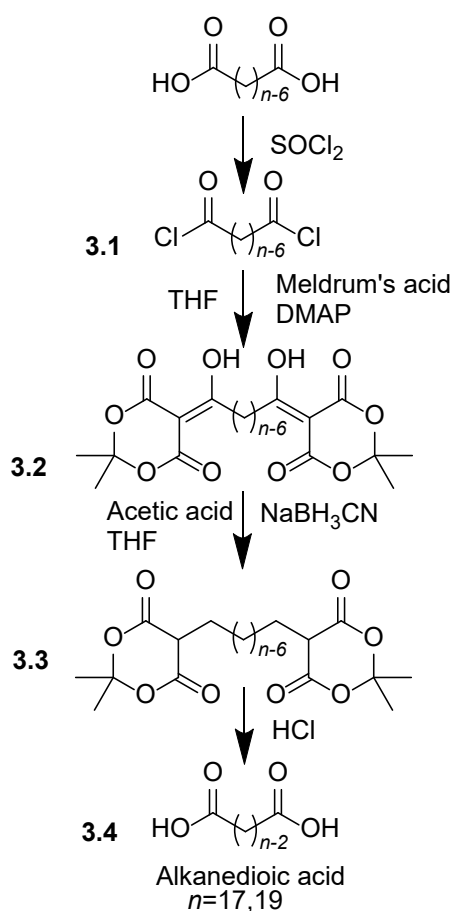
$\delta_{\text{H}}/\text{ppm}$ (400 MHz, CDCl_3): 7.74 (4 H, d, J 8.2 Hz, Ar-H), 7.70 (4 H, d, J 8.2 Hz, Ar-H), 7.56 (4 H, d, J 7.8 Hz, Ar-H), 7.34 (4 H, d, J 7.8 Hz, Ar-H), 2.77 (4 H, t, J 7.7 Hz, Ar-CH₂-CH₂-), 2.07 (2 H, quin, J 7.7 Hz, Ar-CH₂-CH₂-CH₂-)

$\delta_{\text{C}}/\text{ppm}$ (100 MHz, CDCl_3): 145.49, 142.89, 136.76, 132.59, 129.22, 127.50, 127.20, 119.00, 110.66, 35.06, 32.72

EA: Calculated for $\text{C}_{29}\text{H}_{22}\text{N}_2$: C = 87.41 %, H = 5.56 %, N = 7.03 %; Found: C = 86.91 %, H = 5.64 %, N = 6.83 %

MS (ESI+, m/z) = $[\text{M}+\text{Na}]^+$: Calculated for $\text{C}_{29}\text{H}_{22}\text{N}_2\text{Na}$: 421.1681; Found: 421.1673. Difference: 1.9 ppm.

Extended Alkanedioic Acids



Scheme S13. Synthesis of extended alkanedioic acids.

The synthesis of the alkanedioic acids follows the steps outlined in **Scheme S13**. The alkanedioic acids (**3.4**) were synthesised using a method described by Obaza and Smith.⁶ The starting alkanedioic acid was converted to an acid chloride before acylating Meldrum's acid. This was followed by a hydride reduction and then subsequently, the acid hydrolysis and decarboxylation of the ester to form the desired product.

3.1 Alkanedioyl chlorides

To a pre-dried flask flushed with argon, the starting alkanedioic acid (1 eq) of an appropriate chain length was added. The acid was then azeotroped with dry toluene (2×15 mL) and once dried, thionyl chloride (5.2 eq) was added with stirring. The quantities of the reagents used in each reaction are listed in **Table S11**. The mixture was heated to 70 °C for 2 h which generated a yellow/brown liquid. The excess of thionyl chloride remaining in the flask was removed using high vacuum. To ensure all the thionyl chloride had been removed, dry toluene (1×10 mL)

was added to the flask before also being removed under high vacuum. The yellow/brown liquid remaining was then used without any further purification.

Table SII. Quantities of reagents used in the preparation of alkanedioyl chlorides (**3.1**).

<i>n</i>	Alkanedioic acid	Thionyl chloride
17	5.21 g, 0.0213 mol	8.0 mL, 13.1 g, 0.110 mol
19	8.39 g, 0.0308 mol	11.6 mL, 19.1 g, 0.160 mol

3.1.1 *Tridecanedioyl chloride*

Yield: 5.94 g, 99.1 %

3.1.2 *Pentadecanedioyl chloride*

Yield: 9.33 g, 98.2 %

3.2 5-(ω -(2,2-Dimethyl-4,6-dioxo-1,3-dioxan-5-ylidene)-1, ω -dihydroxyalkylidene)-2,2-dimethyl-1,3-dioxane-4,6-diones

To a pre-dried flask flushed with argon, 4-dimethylaminopyridine (2.77 eq) and 2,2-dimethyl-1,3-dioxane-4,6-dione (4.08 eq) were added. The solids were azeotroped with dry toluene (1 \times 50 mL) and once dried, dry tetrahydrofuran (45 mL) was added. The resulting mixture was then stirred while compound **3.1** (1 eq) prepared previously was added dropwise. The quantities of the reagents used in each reaction are listed in **Table SI2**. Following the addition of the reactants, the reaction was left overnight at room temperature, and the extent of the reaction was monitored by TLC using 50 % hexane and 50 % ethyl acetate as the solvent system (RF values quoted in the product data). Water (288 mL) was added to the viscous yellow liquid formed to quench any remaining acid chloride, before 6 M hydrochloric acid (50 mL) was used to adjust the pH of the mixture to 1. The organic solvent in the flask was removed under reduced pressure and a yellow precipitate formed in the remaining aqueous layer, which was collected by vacuum filtration. The crude product obtained was recrystallised from hot methanol (100 mL) to give the desired compound as a white solid.

Table S12. Quantities of reagents used in the preparation of 5-(ω -(2,2-dimethyl-4,6-dioxo-1,3-dioxan-5-ylidene)-1, ω -dihydroxyalkylidene)-2,2-dimethyl-1,3-dioxane-4,6-diones (**3.2**).

<i>n</i>	(3.1)	4-Dimethylaminopyridine	2,2-Dimethyl-1,3-dioxane-4,6-dione
17	5.94 mL, 5.94 g, 0.0211 mol	7.13 g, 0.0584 mol	12.4 g, 0.0861 mol
19	9.33 mL, 9.33 g, 0.0302 mol	10.2 g, 0.0837 mol	17.7 g, 0.123 mol

3.2.1 **5-(13-(2,2-Dimethyl-4,6-dioxo-1,3-dioxan-5-ylidene)-1,13-dihydroxytridecylidene)-2,2-dimethyl-1,3-dioxane-4,6-dione**

Yield: 9.14 g, 87.2 %. RF: 0.57. MP: 158 °C

ν_{max}/cm^{-1} : 2919, 2854, 1729, 1650, 1569, 1413, 1393, 1294, 1267, 1200, 1148, 1026, 955, 913, 801, 732, 722, 645

δ_H/ppm (400 MHz, $CDCl_3$): 15.31 (2 H, s, OH), 3.08 (4 H, t, J 7.7 Hz, C(OH)-CH₂-CH₂-), 1.75 (16 H, m, O-C-CH₃, C(OH)-CH₂-CH₂-CH₂-), 1.41 (4 H, quin, J 7.3 Hz, C(OH)-CH₂-CH₂-CH₂-CH₂-), 1.32 (10 H, m, C(OH)-CH₂-CH₂-CH₂-CH₂-CH₂-CH₂-CH₂-)

δ_C/ppm (100 MHz, $CDCl_3$): 198.32, 170.59, 160.19, 104.77, 91.24, 35.76, 30.95, 29.48, 29.37, 29.21, 26.82, 26.15

Data consistent with reported values ⁷

3.2.2 **5-(15-(2,2-Dimethyl-4,6-dioxo-1,3-dioxan-5-ylidene)-1,15-dihydroxypentadecylidene)-2,2-dimethyl-1,3-dioxane-4,6-dione**

Yield: 14.09 g, 88.7 %. RF: 0.52. MP: 160 °C

ν_{max}/cm^{-1} : 2919, 2854, 1729, 1729, 1651, 1571, 1415, 1394, 1294, 1271, 1201, 1150, 1026, 957, 914, 802, 732, 721, 646

δ_H/ppm (400 MHz, $CDCl_3$): 15.31 (2 H, s, OH), 3.08 (4 H, t, J 7.7 Hz, C(OH)-CH₂-CH₂-), 1.75 (16 H, m, O-C-CH₃, C(OH)-CH₂-CH₂-), 1.41 (4 H, quin, J 7.3 Hz, C(OH)-CH₂-CH₂-CH₂-CH₂-), 1.29 (14 H, m, C(OH)-CH₂-CH₂-CH₂-CH₂-CH₂-CH₂-CH₂-CH₂-)

δ_C/ppm (100 MHz, $CDCl_3$): 198.34, 170.59, 160.20, 104.77, 91.24, 35.78, 29.58, 29.56, 29.43, 29.39, 29.24, 26.83, 26.16

EA: Calculated for $C_{27}H_{40}O_{10}$: C = 61.82 %, H = 7.69 %, O = 30.50 %. Found: C = 61.79 %, H = 7.92 %

3.3 1, ω -Bis(2,2-dimethyl-4,6-dioxo-1,3-dioxan-5-yl)alkanes

To a pre-dried flask flushed with argon, compound **3.2** (1 eq) was added and dissolved in a mixture of glacial acetic acid and tetrahydrofuran. To the resultant solution, sodium cyanoborohydride (2.20 eq) was added. The quantities of the reagents used in each reaction are listed in **Table SI3**. The mixture was left at room temperature to stir for 5 minutes, heated to 60 °C for 2 h and monitored by TLC using 50 % hexane and 50 % ethyl acetate as the solvent system (RF values quoted in the product data). The reaction was cooled to room temperature and poured into a beaker containing water (500 mL). Upon addition the mixture was rapidly stirred to generate a white precipitate and hydrochloric acid (40 mL) was added. The precipitate was collected using vacuum filtration and this was recrystallised from hot ethanol (150 mL) to give the desired product as a white solid.

Table SI3. Quantities of reagents used in the preparation of 1, ω -bis(2,2-dimethyl-4,6-dioxo-1,3-dioxan-5-yl)alkanes (**3.3**).

<i>n</i>	(3.2)	Sodium cyanoborohydride	Glacial acetic acid	Tetrahydrofuran
17	7.99 g, 0.0161 mol	2.23 g, 0.0354 mol	64 mL	95 mL
19	10.1 g, 0.0192 mol	2.65 g, 0.0422 mol	80 mL	116 mL

3.3.1 1,13-Bis(2,2-dimethyl-4,6-dioxo-1,3-dioxan-5-yl)tridecane

Yield: 6.50 g, 86.3 %. RF: 0.67. MP: 143 °C

ν_{max}/cm^{-1} : 2917, 2850, 1738, 1382, 1332, 1311, 1205, 1059, 981, 878

$\delta_{\text{H}}/\text{ppm}$ (400 MHz, CDCl_3): 3.49 (2 H, t, J 5.0 Hz, (C=O)-CH-CH₂-), 2.09 (4 H, m, (C=O)-CH-CH₂-CH₂-), 1.78 (6 H, s, O-C-CH₃), 1.75 (6 H, s, O-C-CH₃), 1.27 (22 H, m, (C=O)-CH-CH₂-CH₂-CH₂-CH₂-CH₂-CH₂-CH₂-)

$\delta_{\text{C}}/\text{ppm}$ (100 MHz, CDCl_3): 165.71, 104.80, 46.16, 29.56, 29.54, 29.51, 29.49, 29.25, 28.46, 26.98, 26.70, 26.55

Data consistent with reported values ⁷

3.3.2 1,15-Bis(2,2-dimethyl-4,6-dioxo-1,3-dioxan-5-yl)pentadecane

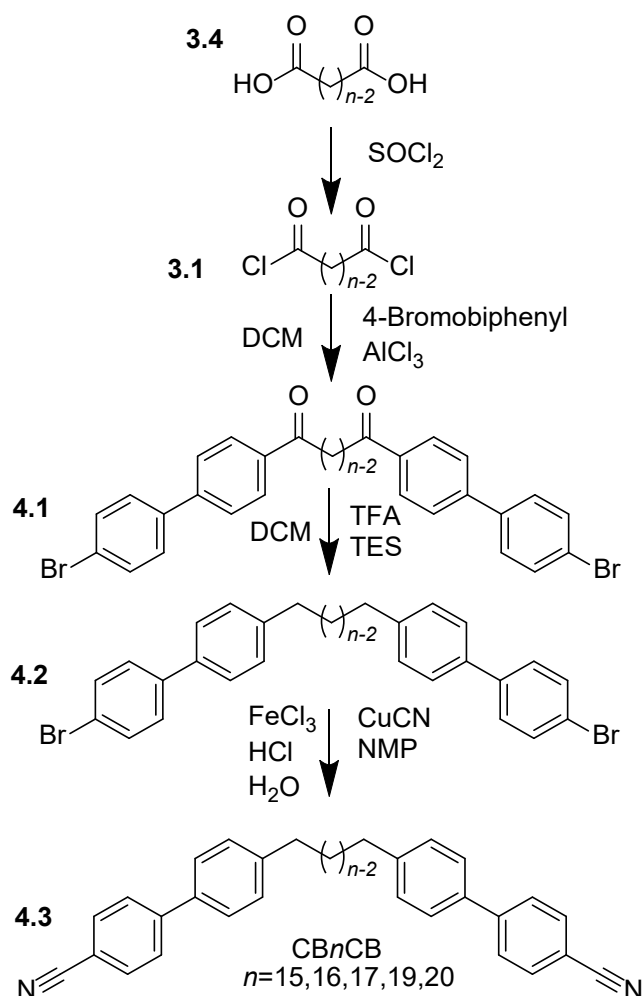
Yield: 8.96 g, 94.0 %. RF: 0.62. MP: 144 °C

ν_{max}/cm^{-1} : 2917, 2850, 1738, 1382, 1332, 1311, 1205, 1059, 981, 878

δ_C /ppm (100 MHz, CDCl_3): 180.28, 34.06, 29.58, 29.53, 29.50, 29.44, 29.35, 29.15, 28.99, 24.65

Data consistent with reported values ⁸

CB_nCB Series



Scheme SI4. Synthesis of the CB_nCB series.

The synthesis of the CB_nCB series follows the steps outlined in **Scheme SI4**. The CB_nCB series (**4.3**) was synthesised using a method described by Paterson *et al.*¹ The alkanedioic acid (**3.4**) was converted to an acid chloride before it underwent a Friedel-Crafts acylation and a subsequent hydrosilane reduction. This was followed by a modified Rosenmund-von Braun cyanation reaction to form the desired product.

3.1 Alkanedioyl chlorides

To a pre-dried flask flushed with argon, compound **3.4** (1 eq) was added. The acid was then azeotroped with dry toluene (2×15 mL) and once all the toluene had been removed, thionyl chloride (10 eq) was added and then stirred. The quantities of the reagents used in each reaction are listed in **Table SI5**. The mixture was heated to 70 °C for 2 h which generated a yellow/brown liquid. The excess of thionyl chloride remaining in the flask was removed using high vacuum. To ensure all the thionyl chloride had been removed dry toluene (1×10 mL) was added to the flask before also being removed under high vacuum. The yellow/brown liquid remaining was then used without any further purification.

Table SI5. Quantities of reagents used in the preparation of alkanedioyl chlorides (**3.1**).

<i>n</i>	(3.4)	Thionyl chloride
15	2.00 g, 7.34×10^{-3} mol	5.35 mL, 8.73 g, 0.0734 mol
16	2.51 g, 8.76×10^{-3} mol	6.35 mL, 10.4 g, 0.0876 mol
17	4.68 g, 0.0156 mol	11.3 mL, 18.6 g, 0.156 mol
19	4.49 g, 0.0137 mol	9.94 mL, 16.3 g, 0.137 mol
20	5.07 g, 0.0148 mol	10.7 mL, 17.6 g, 0.148 mol

3.1.3 *Pentadecanedioyl chloride*

Yield: 2.16 g, 95.2 %

3.1.4 *Hexadecanedioyl chloride*

Yield: 2.81 g, 99.2 %

3.1.5 *Heptadecanedioyl chloride*

Yield: 5.16 g, 98.0 %

3.1.6 *Nonadecanedioyl chloride*

Yield: 4.93 g, 98.4 %

3.1.7 *Eicosanedioyl chloride*

Yield: 5.55 g, 98.8 %

4.1 1, ω -Bis-(4'-bromo-[1,1'-biphenyl]-4-yl)alkane-1, ω -diones

To a pre-dried flask flushed with argon, aluminium chloride (2.20 eq, 2.35 eq for $n = 15$) was added along with dry dichloromethane (60 mL, 30 mL for $n = 15$) while being stirred. The outside of the flask was wrapped in aluminium foil to prevent light from interfering with the reaction and placed into an ice bath in order to keep the reaction mixture at 0 °C. 4-Bromobiphenyl (2 eq) and compound **3.1** (1 eq) were mixed along with dry dichloromethane (60 mL, 30 mL for $n = 15$) before being added dropwise into the flask. The quantities of the reagents used in each reaction are listed in **Table SI6**. The ice bath was removed, and the reaction was left to stir at room temperature overnight. The extent of the reaction was monitored by TLC using dichloromethane as the solvent system (RF values quoted in the product data). The resultant mixture was added to a slurry of ice (50 g) with 6 M hydrochloric acid (12 mL) and extracted with dichloromethane (200 mL). The extracted organic layer was washed with water (3 \times 50 mL) and dried over anhydrous magnesium sulfate. The magnesium sulfate was removed using vacuum filtration and the solvent evaporated under vacuum to leave an orange solid which was recrystallised from hot toluene (70 mL, 40 mL for $n = 15$).

Table 3.1.6. Quantities of reagents used in the preparation of 1, ω -bis-(4'-bromobiphenyl-4-yl)alkane-1, ω -diones (**4.1**).

n	(3.1)	4-Bromobiphenyl	Aluminium chloride
15	1.21 mL, 1.21 g, 3.91×10^{-3} mol	1.84 g, 7.89×10^{-3} mol	1.23 g, 9.22×10^{-3} mol
16	2.81 mL, 2.81 g, 8.69×10^{-3} mol	4.06 g, 0.0174 mol	2.55 g, 0.0191 mol
17	5.16 mL, 5.16 g, 0.0153 mol	7.13 g, 0.0306 mol	4.49 g, 0.0337 mol
19	4.93 mL, 4.93 g, 0.0135 mol	6.29 g, 0.0270 mol	3.96 g, 0.0297 mol
20	5.55 mL, 5.55 g, 0.0146 mol	6.80 g, 0.0292 mol	4.28 g, 0.0321 mol

4.1.1 1,15-Bis-(4'-bromo-[1,1'-biphenyl]-4-yl)pentadecane-1,15-dione

White solid. Yield: 1.60 g, 58.2 %. RF: 0.52. MP: 174 °C

ν_{max}/cm^{-1} : 2912, 2847, 1673, 1586, 1481, 1472, 1002, 804

$\delta_{\text{H}}/\text{ppm}$ (400 MHz, CDCl_3): 8.03 (4 H, d, J 8.2 Hz, Ar-H), 7.66 (4 H, d, J 8.2 Hz, Ar-H), 7.60 (4 H, d, J 8.5 Hz, Ar-H), 7.49 (4 H, d, J 8.5 Hz, Ar-H), 2.99 (4 H, t, J 7.4 Hz, C(=O)-CH₂-CH₂-), 1.75 (4 H, quin, J 7.4 Hz, (C=O)-CH₂-CH₂-CH₂-), 1.30 (18 H, m, C(=O)-CH₂-CH₂-CH₂-CH₂-CH₂-CH₂-CH₂-)

$\delta_{\text{C}}/\text{ppm}$ (100 MHz, CDCl_3): 200.09, 144.25, 138.85, 136.10, 132.09, 128.81, 128.77, 127.02, 122.60, 38.73, 29.62, 29.60 (2 \times C), 29.50, 29.40, 24.45

4.1.2 *1,16-Bis-(4'-bromo-[1,1'-biphenyl]-4-yl)hexadecane-1,16-dione*

Orange solid. Yield: 3.54 g, 56.8 %. RF: 0.59. MP: 170 °C

ν_{max}/cm^{-1} : 2917, 2854, 1679, 1588, 1472, 1464, 1387, 1335, 1296, 1212, 1184, 1083, 1002, 812, 762, 732, 721, 646, 574

$\delta_{\text{H}}/\text{ppm}$ (400 MHz, CDCl_3): 8.03 (4 H, d, J 8.0 Hz, Ar-H), 7.64 (4 H, d, J 8.0 Hz, Ar-H), 7.60 (4 H, d, J 8.2 Hz, Ar-H), 7.49 (4 H, d, J 8.2 Hz, Ar-H), 2.98 (4 H, t, J 7.4 Hz, C(=O)-CH₂-CH₂-), 1.74 (4 H, quin, J 7.4 Hz, (C=O)-CH₂-CH₂-CH₂-), 1.29 (20 H, m, C(=O)-CH₂-CH₂-CH₂-CH₂-CH₂-CH₂-CH₂-)

$\delta_{\text{C}}/\text{ppm}$ (100 MHz, CDCl_3): 200.09, 144.24, 138.85, 136.10, 132.09, 128.81, 128.77, 127.01, 122.60, 38.74, 29.66 (2 × C), 29.63, 29.52, 29.41, 24.46

4.1.3 *1,17-Bis-(4'-bromo-[1,1'-biphenyl]-4-yl)heptadecane-1,17-dione*

Orange solid. Yield: 2.47 g, 22.1 %. RF: 0.52. MP: 150 °C

ν_{max}/cm^{-1} : 2914, 2848, 1675, 1604, 1587, 1484, 1464, 1374, 1206, 1183, 1084, 1002, 813, 804, 776, 665, 575

$\delta_{\text{H}}/\text{ppm}$ (400 MHz, CDCl_3): 8.03 (4 H, d, J 8.0 Hz, Ar-H), 7.65 (4 H, d, J 8.0 Hz, Ar-H), 7.60 (4 H, d, J 8.0 Hz, Ar-H), 7.49 (4 H, d, J 8.0 Hz, Ar-H), 2.99 (4 H, t, J 7.4 Hz, C(=O)-CH₂-CH₂-), 1.76 (4 H, quin, J 7.4 Hz, (C=O)-CH₂-CH₂-CH₂-), 1.25 (22 H, m, C(=O)-CH₂-CH₂-CH₂-CH₂-CH₂-CH₂-CH₂-CH₂-)

$\delta_{\text{C}}/\text{ppm}$ (100 MHz, CDCl_3): 200.09, 144.24, 138.83, 136.10, 132.10, 128.81, 128.75, 127.02, 122.60, 38.74, 29.71 (2 × C), 29.64, 29.61, 29.57, 29.40, 24.45

4.1.4 *1,19-Bis-(4'-bromo-[1,1'-biphenyl]-4-yl)nonadecane-1,19-dione*

Off-white solid. Yield: 3.17 g, 31.0 %. RF: 0.50. MP: 160 °C

ν_{max}/cm^{-1} : 2914, 2848, 1675, 1587, 1604, 1588, 1472, 1388, 1204, 1182, 1084, 1002, 985, 813, 804, 776, 762, 719, 665, 575

$\delta_{\text{H}}/\text{ppm}$ (400 MHz, CDCl_3): 8.05 (4 H, d, J 8.1 Hz, Ar-H), 7.66 (4 H, d, J 8.1 Hz, Ar-H), 7.62 (4 H, d, J 8.2 Hz, Ar-H), 7.51 (4 H, d, J 8.2 Hz, Ar-H), 3.01 (4 H, t, J 7.4 Hz, C(=O)-CH₂-CH₂-), 1.77 (4 H, quin, J 7.4 Hz, (C=O)-CH₂-CH₂-CH₂-), 1.28 (26 H, m, C(=O)-CH₂-CH₂-CH₂-CH₂-CH₂-CH₂-CH₂-CH₂-CH₂-)

$\delta_{\text{C}}/\text{ppm}$ (100 MHz, CDCl_3): 200.12, 144.25, 138.85, 136.10, 132.09, 128.81, 128.77, 127.02, 122.60, 38.74, 29.68 (2 × C), 29.67, 29.64, 29.52, 29.50, 29.41, 24.46

4.1.5 *1,20-Bis-(4'-bromo-[1,1'-biphenyl]-4-yl)icosane-1,20-dione*

Off-white solid. Yield: 5.29 g, 46.8 %. RF: 0.47. MP: 176 °C

ν_{max}/cm^{-1} : 2919, 2849, 1681, 1557, 1471, 1437, 1389, 1082, 1002, 815, 798, 718

$\delta_{\text{H}}/\text{ppm}$ (400 MHz, CDCl_3): 8.03 (4 H, d, J 8.0 Hz, Ar-H), 7.64 (4 H, d, J 8.0 Hz, Ar-H), 7.60 (4 H, d, J 8.3 Hz, Ar-H), 7.49 (4 H, d, J 8.3 Hz, Ar-H), 2.98 (4 H, t, J 7.5 Hz, C(=O)-CH₂-CH₂-), 1.75 (4 H, quin, J 7.5 Hz, (C=O)-CH₂-CH₂-CH₂-), 1.31 (28 H, m, C(=O)-CH₂-CH₂-CH₂-CH₂-CH₂-CH₂-CH₂-CH₂-CH₂-CH₂-)

$\delta_{\text{C}}/\text{ppm}$ (100 MHz, CDCl_3): 200.13, 144.25, 138.84, 136.10, 132.10, 128.81, 128.77, 127.04, 122.61, 38.76, 29.69 (2 × C), 29.68, 29.64, 29.53, 29.52, 29.42, 24.46

4.2 *1,ω-Bis-(4'-bromo-[1,1'-biphenyl]-4-yl)alkanes*

To a pre-dried flask flushed with argon, compound **4.1** (1 eq) was added. The flask was then placed into an ice bath in order to maintain the temperature at 0 °C. The solid was solubilised using trifluoroacetic acid and dry dichloromethane (40 mL), along with stirring. Finally, triethylsilane was added to the flask and the ice bath was removed. The quantities of the reagents used in each reaction are listed in **Table SI7**. The reaction was left for 24 h and the extent of the reaction was monitored by TLC using dichloromethane as the solvent system (RF values quoted in the product data). Once complete, the mixture was added to a beaker with dichloromethane (100 mL) and water (300 mL). The organic layer was separated and washed with water (3 × 50 mL). This was dried using anhydrous magnesium sulfate, which was removed by vacuum filtration, and the solvent evaporated under vacuum to leave an off-white or light orange solid. This solid was recrystallised using a mixture of 50 % hot toluene and 50 % hot ethanol (50 mL, 300 mL for $n = 15$) to give an off white/white or light orange solid.

Table SI7. Quantities of reagents used in the preparation of 1,ω-bis-(4'-bromobiphenyl-4-yl)alkanes (**4.2**).

<i>n</i>	(4.1)	Trifluoroacetic acid	Triethylsilane
15	10.3 g, 0.0146 mol	36.0 mL, 53.6 g, 0.470 mol	26.0 mL, 18.9 g, 0.163 mol
16	2.37 g, 3.31 × 10 ⁻³ mol	25.0 mL, 37.2 g, 0.326 mol	5.0 mL, 3.64 g, 0.0313 mol
17	2.42 g, 3.31 × 10 ⁻³ mol	25.0 mL, 37.2 g, 0.326 mol	5.0 mL, 3.64 g, 0.0313 mol
19	3.05 g, 4.02 × 10 ⁻³ mol	30.0 mL, 44.7 g, 0.392 mol	6.0 mL, 4.37 g, 0.0376 mol
20	5.00 g, 6.92 × 10 ⁻³ mol	50.0 mL, 74.5 g, 0.653 mol	10.0 mL, 7.28 g, 0.0626 mol

4.2.1 *1,15-Bis-(4'-bromo-[1,1'-biphenyl]-4-yl)pentadecane*

White solid. Yield: 6.20 g, 62.9 %. RF: 0.82. MP: 110 °C

ν_{max}/cm^{-1} : 2913, 2848, 1587, 1481, 1471, 1001, 804

$\delta_{\text{H}}/\text{ppm}$ (300 MHz, CDCl_3): 7.56 (4 H, d, J 8.8 Hz, Ar-H), 7.49 (4 H, d, J 8.3 Hz, Ar-H), 7.45 (4 H, d, J 8.8 Hz, Ar-H), 7.26 (4 H, d, J 8.3 Hz, Ar-H), 2.64 (4 H, m, Ar-CH₂-CH₂-), 1.64 (4 H, quin, J 7.3 Hz, Ar-CH₂-CH₂-CH₂-), 1.31 (22 H, m, Ar-CH₂-CH₂-CH₂-CH₂-CH₂-CH₂-CH₂-CH₂-CH₂-)

$\delta_{\text{C}}/\text{ppm}$ (75 MHz, CDCl_3): 142.60, 140.08, 137.27, 131.79, 128.96, 128.55, 126.76, 121.15, 35.62, 31.49, 29.68 (2 × C), 29.64, 29.61, 29.54, 29.37

4.2.2 *1,16-Bis-(4'-bromo-[1,1'-biphenyl]-4-yl)hexadecane*

Light orange solid. Yield: 0.955 g, 58.6 %. RF: 0.85. MP: 114 °C

ν_{max}/cm^{-1} : 2917, 2847, 1588, 1481, 1462, 1390, 1079, 1002, 821, 800, 757, 723, 695, 491, 471

$\delta_{\text{H}}/\text{ppm}$ (400 MHz, CDCl_3): 7.54 (4 H, d, J 8.4 Hz, Ar-H), 7.46 (4 H, d, J 8.4 Hz, Ar-H), 7.43 (4 H, d, J 8.4 Hz, Ar-H), 7.24 (4 H, d, J 8.4 Hz, Ar-H), 2.64 (4 H, t, J 7.5 Hz, Ar-CH₂-CH₂-), 1.74 (4 H, quin, J 7.5 Hz, Ar-CH₂-CH₂-CH₂-), 1.30 (24 H, m, Ar-CH₂-CH₂-CH₂-CH₂-CH₂-CH₂-CH₂-CH₂-CH₂-)

$\delta_{\text{C}}/\text{ppm}$ (100 MHz, CDCl_3): 142.60, 140.09, 137.28, 131.79, 128.96, 128.56, 126.76, 121.15, 35.62, 31.48, 29.69 (2 × C), 29.68, 29.61, 29.53, 29.36

4.2.3 *1,17-Bis-(4'-bromo-[1,1'-biphenyl]-4-yl)heptadecane*

Light orange solid. Yield: 1.45 g, 62.3 %. RF: 0.83. MP: 104 °C

ν_{max}/cm^{-1} : 2915, 2848, 1481, 1471, 1390, 1077, 1002, 807, 762, 718, 694, 491

$\delta_{\text{H}}/\text{ppm}$ (400 MHz, CDCl_3): 7.54 (4 H, d, J 8.0 Hz, Ar-H), 7.46 (4 H, d, J 8.4 Hz, Ar-H), 7.43 (4 H, d, J 8.0 Hz, Ar-H), 7.24 (4 H, d, J 8.4 Hz, Ar-H), 2.64 (4 H, t, J 7.7 Hz, Ar-CH₂-CH₂-), 1.64 (4 H, quin, J 7.7 Hz, Ar-CH₂-CH₂-CH₂-), 1.27 (26 H, m, Ar-CH₂-CH₂-CH₂-CH₂-CH₂-CH₂-CH₂-CH₂-CH₂-)

$\delta_{\text{C}}/\text{ppm}$ (100 MHz, CDCl_3): 142.60, 140.09, 137.28, 131.78, 128.96, 128.55, 126.76, 121.15, 35.62, 31.48, 29.68 (3 × C), 29.67, 29.60, 29.53, 29.36

4.2.4 *1,19-Bis-(4'-bromo-[1,1'-biphenyl]-4-yl)nonadecane*

Off-white solid. Yield: 2.17 g, 74.0 %. RF: 0.81. MP: 100 °C

ν_{max}/cm^{-1} : 2915, 2848, 1482, 1471, 1390, 1079, 1002, 805, 793, 717, 492, 481

(RF values quoted in product data). The eluent fractions of interest were evaporated under vacuum to leave a white solid which was recrystallised from hot ethanol (40 mL).

Table SI8. Quantities of reagents used in the preparation of 1, ω -bis-(4'-cyano-[1,1'-biphenyl]-4-yl)alkanes (**4.3**).

<i>n</i>	(4.2)	Copper (I) cyanide	Iron (III) Chloride
15	1.00 g, 1.48×10^{-3} mol	0.530 g, 5.92×10^{-3} mol	1.91 g, 0.0118 mol
16	0.935 g, 1.36×10^{-3} mol	0.486 g, 5.43×10^{-3} mol	1.77 g, 0.0109 mol
17	1.40 g, 1.99×10^{-3} mol	0.712 g, 7.95×10^{-3} mol	2.58 g, 0.0159 mol
19	1.49 g, 2.04×10^{-3} mol	0.731 g, 8.16×10^{-3} mol	2.64 g, 0.0163 mol
20	1.50 g, 2.01×10^{-3} mol	0.722 g, 8.06×10^{-3} mol	2.61 g, 0.0161 mol
	Hydrochloric Acid	Water	
15	1.82 mL, 2.12 g, 0.0592 mol	5.0 mL	
16	1.70 mL, 1.98 g, 0.0544 mol	5.0 mL	
17	2.51 mL, 2.91 g, 0.0795 mol	7.0 mL	
19	2.56 mL, 2.97 g, 0.0815 mol	7.0 mL	
20	2.53 mL, 2.93 g, 0.0804 mol	7.0 mL	

4.3.1 *1,15-Bis-(4'-cyano-[1,1'-biphenyl]-4-yl)pentadecane (CB15CB)*

Yield: 0.240 g, 28.6 %. RF: 0.46

$T_{CrN_{TB}}$ 95 °C $T_{N_{TBN}}$ 103 °C T_{NI} 121 °C

ν_{max}/cm^{-1} : 2918, 2848, 2225, 1604, 1467, 1004, 809

δ_H/ppm (400 MHz, $CDCl_3$): 7.72 (4 H, d, J 8.5 Hz, Ar-H), 7.68 (4 H, d, J 8.5 Hz, Ar-H), 7.53 (4 H, d, J 8.3 Hz, Ar-H), 7.31 (4 H, d, J 8.3 Hz, Ar-H), 2.68 (4 H, t, J 7.8 Hz, Ar-CH₂-CH₂-), 1.67 (4 H, quin, J 7.8 Hz, Ar-CH₂-CH₂-CH₂-), 1.30 (22 H, m, Ar-CH₂-CH₂-CH₂-CH₂-CH₂-CH₂-CH₂-)

δ_C/ppm (100 MHz, $CDCl_3$): 145.62, 143.81, 136.44, 132.57, 129.19, 127.48, 127.07, 119.07, 110.50, 35.65, 31.44, 29.69 (2 × C), 29.61, 29.53, 29.34

MS (ESI+, m/z) = $[M+Na]^+$: Calculated for $C_{41}H_{46}N_2Na$: 589.3559; Found: 589.3550.

Difference: 1.5 ppm.

4.3.2 *1,16-Bis-(4'-cyano-[1,1'-biphenyl]-4-yl)hexadecane (CB16CB)*

Yield: 0.211 g, 26.7 %. RF: 0.52

T_{CrN} 111 °C T_{NI} 132 °C

5.1 4',4''-[1, ω -Alkanediylbis(oxy)]bis-[1,1'-biphenyl]-4-carbonitriles (CBO n OCB)

To a pre-dried flask flushed with argon and fitted with a condenser, 4'-hydroxy-4-biphenylcarbonitrile (2 eq) and potassium carbonate (4 eq) were added. Cyclohexane (30 mL) was added with the appropriate 1, ω -dibromoalkane (1 eq) and stirred. The quantities of the reagents used in each reaction are listed in **Table SI9**. The reaction was refluxed overnight, and the extent of the reaction was monitored by TLC using dichloromethane as the solvent system (RF values quoted in the product data). The reaction mixture was cooled to room temperature and poured into water (150 mL). The resulting white precipitate was vacuum filtered and recrystallised from hot ethyl acetate (30 mL).

Table SI9. Quantities of reagents used in the syntheses of 4',4''-[1, ω -alkanediylbis(oxy)]bis-[1,1'-biphenyl]-4-carbonitriles (**5.1**).

<i>n</i>	1, ω -Dibromoalkane	4'-Hydroxy-4-biphenylcarbonitrile	Potassium carbonate
1	0.36 mL, 0.88 g, 5.10×10^{-3} mol	2.00 g, 1.02×10^{-2} mol	2.83 g, 2.05×10^{-2} mol
7	0.85 mL, 1.27 g, 4.93×10^{-3} mol	1.92 g, 9.86×10^{-3} mol	2.73 g, 1.97×10^{-2} mol
9	1.02 mL, 1.43 g, 5.00×10^{-3} mol	2.76 g, 1.00×10^{-2} mol	2.76 g, 2.00×10^{-2} mol
11	1.76 mL, 2.36 g, 7.50×10^{-3} mol	2.93 g, 1.50×10^{-2} mol	4.15 g, 3.00×10^{-2} mol

5.1.1 4',4''-[1,1-Methanediylbis(oxy)]bis-[1,1'-biphenyl]-4-carbonitriles (CBO1OCB)

Yield: 1.32 g, 64.3 %. RF: 0.49

T_{CH} 149 °C T_{NI} (104 °C)

ν_{max}/cm^{-1} : 2223, 1602, 1518, 1491, 1288, 1217, 1175, 1149, 1029, 1009, 997, 848, 816, 805, 562, 530

$\delta_{\text{H}}/\text{ppm}$ (400 MHz, CDCl₃): 7.70 (4 H, d, J 8.1 Hz, Ar-H), 7.64 (4 H, d, J 8.1 Hz, Ar-H), 7.56 (4 H, d, J 8.3 Hz, Ar-H), 7.24 (4 H, d, J 8.3 Hz, Ar-H), 5.84 (2 H, s, O-CH₂-O)

$\delta_{\text{C}}/\text{ppm}$ (100 MHz, CDCl₃): 157.33, 144.96, 133.52, 132.63, 128.54, 127.30, 118.98, 116.96, 110.54, 90.80

EA: Calculated for C₂₇H₁₈N₂O₂: C = 80.58 %, H = 4.51 %, N = 6.96 %; Found: C = 80.48 %, H = 4.62 %, N = 6.89 %

5.1.3 4',4''-[1,7-Heptanediylbis(oxy)]bis-[1,1'-biphenyl]-4-carbonitriles (CBO7OCB)

Yield: 1.29 g, 53.8 %. RF: 0.38

T_{CHN} 138 °C T_{N_{TB}N} (85 °C) T_{NI} 181 °C

ν_{max}/cm^{-1} : 2942, 2856, 2218, 1604, 1518, 1494, 1472, 1395, 1292, 1244, 1174, 1112, 1034, 998, 820, 803, 737, 660, 564, 531

$\delta_{\text{H}}/\text{ppm}$ (400 MHz, CDCl_3): 7.69 (4 H, d, J 8.3 Hz, Ar-H), 7.64 (4 H, d, J 8.3 Hz, Ar-H), 7.53 (4 H, d, J 8.6 Hz, Ar-H), 6.99 (4 H, d, J 8.6 Hz, Ar-H), 4.02 (4 H, t, J 6.5 Hz, O-CH₂-CH₂-), 1.85 (4 H, tt, J 7.2 Hz, 6.5 Hz, O-CH₂-CH₂-CH₂-), 1.51 (6 H, m, O-CH₂-CH₂-CH₂-CH₂-CH₂-)

$\delta_{\text{C}}/\text{ppm}$ (100 MHz, CDCl_3): 159.75, 145.25, 132.58, 131.32, 128.35, 127.08, 119.13, 115.07, 110.06, 68.07, 29.18, 29.15, 26.02

Data consistent with reported values.^{9,10}

5.1.4 **4',4''-[1,9-Nonanediylbis(oxy)]bis-[1,1'-biphenyl]-4-carbonitriles** **(CBO9OCB)**

Yield: 1.47 g, 57.1 %. RF: 0.38

T_{CrN} 135 °C $T_{\text{N}_{\text{TBN}}}$ (81 °C) T_{NI} 172 °C

ν_{max}/cm^{-1} : 2925, 2855, 2223, 1601, 1579, 1522, 1494, 1396, 1292, 1269, 1249, 1176, 1032, 1012, 814, 724, 661, 563, 530

$\delta_{\text{H}}/\text{ppm}$ (400 MHz, CDCl_3): 7.69 (4 H, d, J 8.5 Hz, Ar-H), 7.63 (4 H, d, J 8.5 Hz, Ar-H), 7.53 (4 H, d, J 8.8 Hz, Ar-H), 6.99 (4 H, d, J 8.8 Hz, Ar-H), 4.01 (4 H, t, J 6.5 Hz, O-CH₂-CH₂-), 1.82 (4 H, tt, J 6.9 Hz, 6.5 Hz, O-CH₂-CH₂-CH₂-), 1.49 (4 H, tt, J 6.9 Hz, 6.4 Hz, O-CH₂-CH₂-CH₂-CH₂-), 1.38 (6 H, m, O-CH₂-CH₂-CH₂-CH₂-CH₂-CH₂-)

$\delta_{\text{C}}/\text{ppm}$ (100 MHz, CDCl_3): 159.80, 145.26, 132.57, 131.27, 128.33, 127.07, 119.12, 115.09, 110.06, 68.15, 29.48, 29.32, 29.23, 26.04

Data consistent with reported values.^{9,10}

5.1.5 **4',4''-[1,11-Undecanediylbis(oxy)]bis-[1,1'-biphenyl]-4-carbonitriles** **(CBO11OCB)**

Yield: 1.58 g, 38.9 %. RF: 0.35

T_{CrN} 125 °C $T_{\text{N}_{\text{TBN}}}$ (78 °C) T_{NI} 164 °C

ν_{max}/cm^{-1} : 2938, 2918, 2847, 2223, 1601, 1580, 5121, 1494, 1466, 1394, 1291, 1248, 1178, 1044, 1028, 1009, 1000, 854, 817, 807, 722, 661, 567, 530

$\delta_{\text{H}}/\text{ppm}$ (400 MHz, CDCl_3): 7.69 (4 H, d, J 8.5 Hz, Ar-H), 7.63 (4 H, d, J 8.5 Hz, Ar-H), 7.52 (4 H, d, J 8.8 Hz, Ar-H), 6.99 (4 H, d, J 8.8 Hz, Ar-H), 4.01 (4 H, t, J 6.5 Hz, O-CH₂-CH₂-), 1.81 (4 H, tt, J 7.1 Hz, 6.5 Hz, O-CH₂-CH₂-CH₂-), 1.48 (4 H, tt, J 7.1 Hz, 6.9 Hz, O-CH₂-CH₂-CH₂-CH₂-), 1.35 (10 H, m, O-CH₂-CH₂-CH₂-CH₂-CH₂-CH₂-CH₂-)

$\delta_{\text{C}}/\text{ppm}$ (100 MHz, CDCl_3): 159.80, 145.27, 132.57, 131.27, 128.32, 127.07, 119.11, 115.08, 110.06, 68.18, 29.55, 29.52, 29.39, 29.24, 26.05

Data consistent with reported values.⁹

Trapezium calculations for molecular shape

The shape of the odd-membered dimers of the CB_nCB series can be described as isosceles trapezia due to their symmetry. By drawing the edges of a trapezium onto the model of CB_7CB , see **Figure S11**, the boundaries of the molecular shape can be established. The distance between the nitrogen of the nitrile group and the first atom in the central spacer for one arm of the molecule is given by A. The distance between the nitrogen of the other nitrile group and the first atom in the central spacer for the other arm of the molecule is given by C. In symmetrical dimers, C will be equal to A, but their values will vary when the dimers become non-symmetrical. The distance between the atoms which act as the linking group to connect the chain to the aromatic rings is given by B. The distance between the nitrogen in the nitrile groups is given by D. The angle for the vertex AB is given by X while the angle for the vertex BC is given by X'.

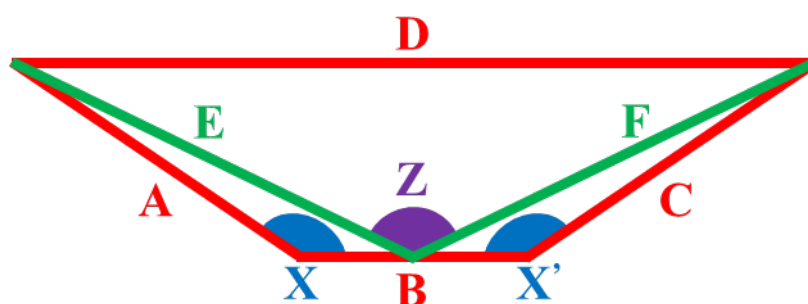


Figure S11. CB_7CB trapezium with all the distances identified to allow the bend angle to be calculated.

The distance between the vertex AD and the midpoint of B is given by E, while the distance between the vertex DC and the midpoint of B is given by F. Much like how A and C have the same value when the molecule is symmetrical, this is also the case for E and F. The bend angle of the molecule is the angle for the vertex EF and is given by Z. The values of A, B, C, D, X and X' could all be found using computational modelling, however E, F and Z could not and so these values were calculated. The distances E and F was calculated using the cosine rule in the form of the following equations respectively:

$$E = \sqrt{A^2 + \left(\frac{B}{2}\right)^2 - AB \cos(X)} \quad (3.1)$$

$$F = \sqrt{C^2 + \left(\frac{B}{2}\right)^2 - CB \cos(X')} \quad (3.2)$$

once E and F were identified a triangle with sides EFD was used in order to find the bend angle for the molecule. Once again, the cosine rule was used to solve the angle Z in the form of the following equation:

$$Z = \cos^{-1} \left(\frac{E^2 + F^2 - D^2}{2EF} \right) \quad (3.3)$$

And the bend angles calculated for the CB_nCB series using this method are listed in **Table SI9**. CB₁CB, due to only having a single carbon in the central spacer, is a triangle rather than a trapezium and so E and F are directly measured in this case.

Table SI9. Calculated bend angles for the odd members of the CB_nCB series.

<i>n</i>	A/ Å	B/ Å	C/ Å	D/ Å	X/ °	X'/ °	E/ Å	F/ Å	Z/ °
1	-	-	-	19.10	-	-	11.26	11.26	116.0
3	11.26	2.57	11.26	21.10	145.4	145.3	12.34	12.34	117.6
5	11.26	5.13	11.26	23.64	145.3	145.3	13.45	13.45	123.0
7	11.26	7.70	11.26	26.21	145.3	145.3	14.59	14.59	127.9
9	11.26	10.26	11.26	28.77	145.3	145.3	15.75	15.75	131.9
11	11.26	12.83	11.26	31.32	145.3	145.3	16.93	16.93	135.3
13	11.26	15.40	11.26	33.87	145.3	145.3	18.13	18.13	138.3
15	11.26	17.96	11.26	36.43	145.3	145.3	19.33	19.33	140.9
17	11.26	20.53	11.26	38.98	145.3	145.3	20.55	20.55	143.1
19	11.26	23.09	11.26	41.54	145.3	145.3	21.77	21.77	145.1

Optical Textures

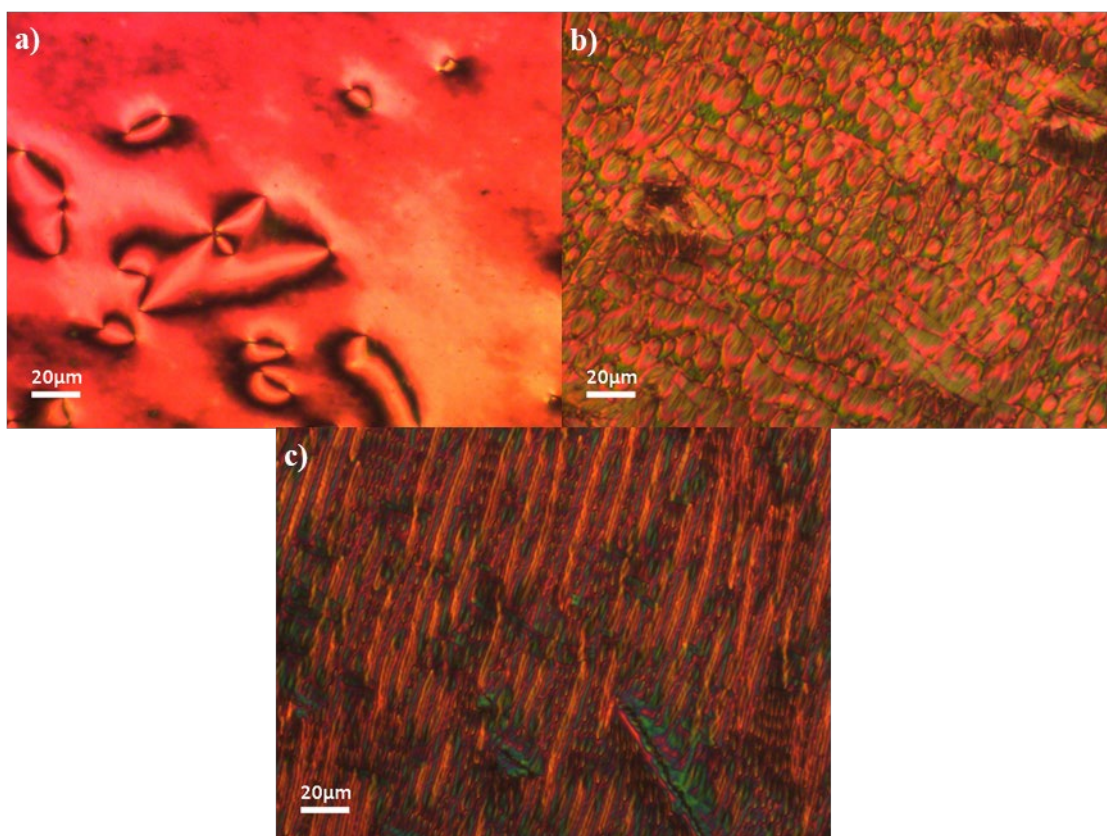


Figure SI2. Textures observed for the 60:40 mol % mixture of CB7CB:CBO10CB: (a) schlieren texture of the nematic phase ($T = 109\text{ }^{\circ}\text{C}$); (b) parabolic texture of the twist-bend nematic phase ($T = 71\text{ }^{\circ}\text{C}$); (c) rope-like texture of the twist-bend nematic phase ($T = 69\text{ }^{\circ}\text{C}$).

References

1. Paterson, D. A., Abberley, J. P., Harrison, W. T. A., Storey, J. M. D. & Imrie, C. T. Cyanobiphenyl-based liquid crystal dimers and the twist-bend nematic phase. *Liq. Cryst.* **44**, 127–146 (2017).
2. Miyaura, N., Yanagi, T. & Suzuki, A. The Palladium-Catalyzed Cross-Coupling Reaction Of Phenylboronic Acid With Haloarenes In The Presence Of Bases. *Synth. Commun.* **11**, 513–519 (1981).
3. Kanagarajan, V., Thanusu, J. & Gopalakrishnan, M. Synthesis and in vitro microbiological evaluation of an array of biolabile 2-morpholino-N-(4,6-diarylpyrimidin-2-yl)acetamides. *Eur. J. Med. Chem.* **45**, 1583–1589 (2010).
4. Chong, J. M., Shen, L. & Taylor, N. J. Asymmetric conjugate addition of alkynylboronates to enones. *J. Am. Chem. Soc.* **122**, 1822–1823 (2000).
5. Akdag, A., Wahab, A., Beran, P., Rulíšek, L., Dron, P. I., Ludvík, J. & Michl, J. Covalent Dimers of 1,3-Diphenylisobenzofuran for Singlet Fission: Synthesis and Electrochemistry. *J. Org. Chem.* **80**, 80–89 (2015).
6. Obaza, J. & Smith, F. X. A Malonic Ester Synthesis with Acid Chlorides. The

- Homologation of Oioic Acids. *Synth. Commun.* **12**, 19–23 (1982).
7. Haulotte, E., Laurent, P. & Braekman, J.-C. Biosynthesis of defensive coccinellidae alkaloids: Incorporation of fatty acids in adaline, coccinelline, and harmonine. *European J. Org. Chem.* **2012**, 1907–1912 (2012).
 8. Walther, G., Deutsch, J., Martin, A., Baumann, F.-E., Fridag, D., Franke, R. & Köckritz, A. α,ω -Functionalized C19 Monomers. *ChemSusChem.* **4**, 1052–1054 (2011).
 9. Emsley, J. W., Luckhurst, G. R., Shilstone, G. N. & Sage, I. The Preparation and Properties of the α,ω -bis(4,4'-Cyanobiphenyloxy)Alkanes: Nematogenic Molecules with a Flexible Core. *Mol. Cryst. Liq. Cryst.* **102**, 223–233 (1984).
 10. Arakawa, Y., Komatsu, K., Shiba, T. & Tsuji, H. Phase behaviors of classic liquid crystal dimers and trimers: Alternate induction of smectic and twist-bend nematic phases depending on spacer parity for liquid crystal trimers. *J. Mol. Liq.* **326**, 115319 (2021).